OPEN ACCESS
IOP Publishing | Songshan Lake Materials Laboratory
Materials Futures
Mater. Futures 2 (2023) 032201 (19pp)
https://doi.org/10.1088/2752-5724/ace1df

Topical Review

# Magnetic skyrmions: materials, manipulation, detection, and applications in spintronic devices

**Huai Zhang[1,4], Yajiu Zhang[2,4], Zhipeng Hou[1,*], Minghui Qin[1], Xingsen Gao[1] and Junming Liu[3]**

[1] Guangdong Provincial Key Laboratory of Optical Information Materials and Technology, Institute for Advanced Materials, South China Academy of Advanced Optoelectronics, South China Normal University, Guangzhou 510006, People's Republic of China
[2] School of Civil Engineering, Guangzhou University, Guangzhou 510006, People's Republic of China
[3] Laboratory of Solid State Microstructures and Innovation Center of Advanced Microstructures, Nanjing University, Nanjing 211102, People's Republic of China

E-mail: houzp@m.scnu.edu.cn

Received 16 April 2023, revised 11 June 2023
Accepted for publication 24 June 2023
Published 25 July 2023

**Abstract**

Magnetic skyrmions are vortex-like spin configurations that possess nanometric dimensions, topological stability, and high controllability through various external stimuli. Since their first experimental observation in helimagnet MnSi in 2009, magnetic skyrmions have emerged as a highly promising candidate for carrying information in future high-performance, low-energy-consumption, non-volatile information storage, and logical calculation. In this article, we provide a comprehensive review of the progress made in the field of magnetic skyrmions, specifically in materials, manipulation, detection, and application in spintronic devices. Firstly, we introduce several representative skyrmion material systems, including chiral magnets, magnetic thin films, centrosymmetric materials, and Van der Waals materials. We then discuss various methods for manipulating magnetic skyrmions, such as electric current and electric field, as well as detecting them, mainly through electrical means such as the magnetoresistance effect. Furthermore, we explore device applications based on magnetic skyrmions, such as track memory, logic computing, and neuromorphic devices. Finally, we summarize the challenges faced in skyrmion research and provide future perspectives.

Keywords: magnetic skyrmions, spintronics, magnetic memory

## 1. Introduction

The rapid development of microelectronic devices in accordance with Moore's law [1], has led to a continuous increase in transistor density on a single chip over the past decades. However, as these devices have become more complex, issues such as power consumption and heat dissipation have become increasingly severe, potentially resulting in the breakdown of Moore's law [2]. In the current research, magnetic

[4] H Zhang and Y J Zhang contributed equally to this work.
[*] Author to whom any correspondence should be addressed.

Original content from this work may be used under the terms of the Creative Commons Attribution 4.0 licence. Any further distribution of this work must maintain attribution to the author(s) and the title of the work, journal citation and DOI.


© 2023 The Author(s). Published by IOP Publishing Ltd on behalf of the Songshan Lake Materials Laboratory

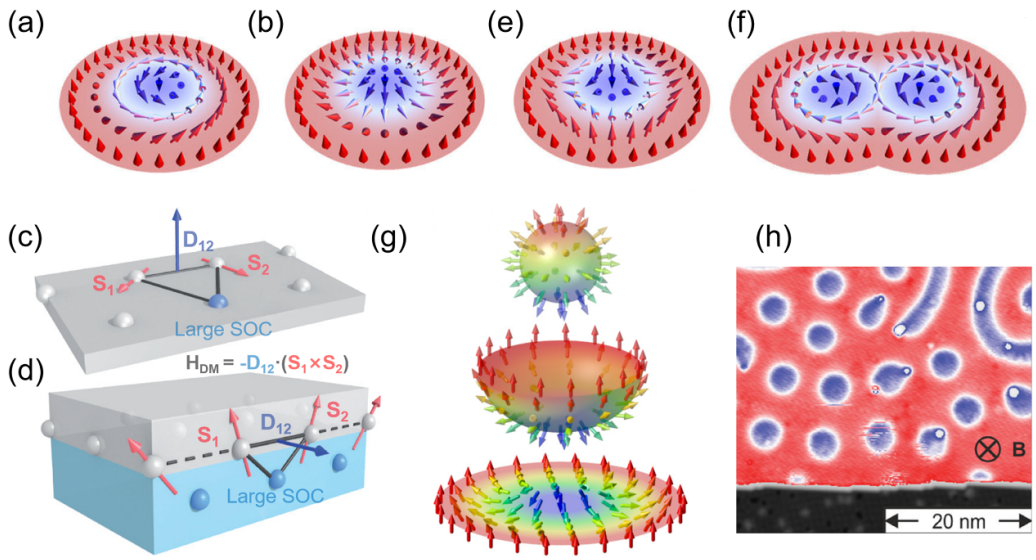


**Figure 1.** Spin configuration of several different types of magnetic skyrmions. (a) Block-type and (b) Néel-type skyrmions with the magnetization rotating from the down direction at the skyrmion's center to the up direction of the external uniform magnetization at the skyrmion's edge. Reproduced from [3]. © IOP Publishing Ltd. All rights reserved. (c) Schematic of DMI in chiral magnet. (d) Schematic illustration of DMI in thin film with asymmetric interface. Reproduced with permission from [7]. Copyright 2013, Springer Nature. Figures (e) and (f) are schematic illustrations of an antiskyrmion and a biskyrmion. Reproduced from [3]. © IOP Publishing Ltd. All rights reserved. (g) Representation of topological charge (top) of the skyrmion (bottom). Reprinted from [11], with the permission of AIP Publishing. (h) Nanoscale skyrmions observed by spin-polarized scanning tunneling microscopy in a monolayer of FePd bilayer grown on Ir(111). Reprinted figure with permission from [27], Copyright (2015) by the American Physical Society.

skyrmions hold promise for carrying information in future high-density, low-dissipation microelectronic devices owing to their nanometric dimensions, topological stability, and low-energy manipulation.

Magnetic skyrmions are topological swirling spin configurations that exhibit unique quasi-particle properties and possess a helical chiral structure (figures 1(a) and (b)) [3]. This structure is characterized by gradual changes in the atomic spin direction from the outer edge to the center, demonstrating a fixed chirality. The chiral structure of a skyrmion is primarily attributed to the Dzyaloshinskii–Moriya interaction (DMI) [4, 5], which is an anti-symmetric exchange interaction between neighboring spins and originates from strong spin–orbit coupling (SOC) in chiral magnets [6, 7] (figure 1(c)) or thin films with the asymmetric interface [7–10] (figure 1(d)). Specifically, the DMI tends to arrange neighboring spin magnetic moments orthogonally, leading to the formation of the chiral spin structure of magnetic skyrmions. The Hamiltonian for DMI can be expressed as follows:

$$H_{\mathrm{DM}} = -\boldsymbol{D}_{ij} \cdot (\boldsymbol{s}_i \times \boldsymbol{s}_j), \tag{1}$$

where $\boldsymbol{s}_i$ and $\boldsymbol{s}_j$ represent the spin of two adjacent atoms, and $\boldsymbol{D}_{ij}$ refers to the DM vector. The magnitude and direction of $\boldsymbol{D}_{ij}$ depend on both the local crystal structure and SOC strength. Due to a delicate interplay between the Heisenberg exchange interaction and DMI, skyrmions can adopt two distinct spin configurations: Bloch-type (figure 1(a)) and Néel-type (figure 1(b)). In Bloch-type skyrmions, the spin rotates along the perpendicular direction of the tangent plane, while in Néel-type skyrmions, they rotate along the parallel direction of the tangent plane. These two configurations can be directly analogous to the two types of magnetic domain walls (DWs).

Compared with conventional ferromagnetic or antiferromagnetic states, magnetic skyrmions exhibit non-trivial topological properties. These properties can be quantified by a topological number, also known as a topological charge (figure 1(g)) [11–14], which is determined by the formula [15]:

$$Q = \frac{1}{4}\int\int \mathrm{d}^2\boldsymbol{r}\boldsymbol{n} \cdot \left(\frac{\partial \boldsymbol{n}}{\partial x} \times \frac{\partial \boldsymbol{n}}{\partial y}\right), \tag{2}$$

where $\boldsymbol{n}$ is the spin unit vector in the $(x, y)$ space. Using the formula (2), one can determine that both Bloch-type and Néel-type magnetic skyrmions have the same topological number ($Q = -1$), suggesting that they are equivalent in topology and can be continuously interconverted through the rotation of spins. Magnetic skyrmions, analogous to particles and antiparticles like electrons and positrons, possess an antiparticle magnetic configuration, known as antiskyrmions. Antiskyrmions exhibit alternating Bloch and Néel-type moment rotations (see figure 1(e)) [3]. These magnetic structures can be stabilized by bulk DMI with lower symmetry, as initially predicted [16, 17], and subsequently experimentally realized in Heusler compounds with $D_{2d}$ symmetry at room temperatures [18]. Antiskyrmions have a topological number opposite to that of magnetic skyrmions (i.e. $Q = 1$) [18, 19]. Notably, Kuchkin *et al* predicted that magnetic topological solitons with opposite values of $Q$, such as skyrmions and antiskyrmions, are expected to be able to continuously merge and annihilate [20]. Recently, the creation and annihilation of skyrmion-antiskyrmion pairs in an

exceptionally thin film of the cubic chiral magnet of B20-type FeGe was observed using transmission electron microscopy [21]. These findings provide a new platform for the fundamental studies of particles and antiparticles based on magnetic solids and open new perspectives for practical applications of thin films of isotropic chiral magnets. Additionally, spins in a class of centrosymmetric magnets can form another configuration, known as biskyrmions (figure 1(f)) [3], which have a topological number of $Q = -2$ [22]. In addition to those above mentioned skyrmions, other spin textures with different topological charges have been identified, including meron ($Q = 1/2$) and antimeron ($Q = -1/2$), which are distinct from skyrmions ($Q = -1$) and antiskyrmions ($Q = 1$). The formation of merons, antimerons, skyrmions, and their lattice structural transitions is expected under increased magnetic anisotropy. Xu recently report the experimental observation of merons and antimerons, as well as the transformation from a square (anti) meron lattice to a hexagonal skyrmion lattice [23]. Additionally, three-dimensional topological spin textures, such as hedgehog ($Q = +1$) and anti-hedgehog ($Q = -1$), also exist. Furthermore, several unique spin configurations have been discovered, including intermediate skyrmion, higher-order skyrmion, bimerons, skyrmioniums, antiferromagnetic skrymion, skyrmion tube, chiral bobber, block-anti-block crystal, hopfion. More comprehensive information on these topologically non-trivial spin textures can be found in recently published review papers on skyrmions [23, 24]. Due to the constancy of the topological number under continuous deformation of the external field, spin configurations with non-zero topological numbers, such as those mentioned above, demonstrate highly stable properties.

The non-trivial topological property of magnetic skyrmions gives them distinctive magnetoelectric coupling properties. Since they have a non-collinear spin structure, magnetic skyrmions give rise to a non-zero Berry phase [24]. As electrons pass through magnetic skyrmions, they induce an extra contribution to the Hall resistance, which is commonly referred to as topological Hall effect (THE). Along with the THE, these also exists a skyrmion Hall effect, that is, the motion of a skyrmion is deflected due to the Magnus force when driven by an electric current [25, 26]. Aside from their innovative physical properties, magnetic skyrmions hold great promise for carrying information in future high-density and low-power-consumption microelectronic devices [7]. Due to their distinctive magnetoelectric coupling, the critical current density for the skyrmion motion is extremely low, at current densities of only $10^6$ A m$^{-2}$, which is about $10^5$–$10^6$ lower than that required to drive traditional magnetic domains or DWs ($10^{11}$–$10^{12}$ A m$^{-2}$) [26]. Furthermore, magnetic skyrmions possess local particle properties, with a size potentially less than 10 nm (figure 1(h)) [27]. Besides, skyrmions exhibit multi-value, controllable and certain randomness characteristics, making them ideal for neural network-related applications [28, 29].

Although current research results indicate that magnetic skyrmions are promising for application in various fields, many challenges must be overcome before magnetic skyrmions can be applied to practical products. Creating a practical skyrmion device requires not only the necessary conditions for magnetic skyrmion materials but also accurate manipulation and detection techniques. This review introduces the progress, challenges and future development perspectives of magnetic skyrmion in the fields of material science, manipulation and detection techniques, and devices based on magnetic skyrmions.

## 2. Development of magnetic skyrmion materials

The concept of skyrmions was originally proposed to explain the stability of hadrons in particle physics [30]. Since then, this model has been found to be applicable in condensed-matter systems (e.g. such as the quantum Hall systems [31, 32], liquid crystals [33], and Bose–Einstein condensates [34]). In 2006, Rößler *et al* predicted the existence of skyrmions in magnetic systems [35]. Following the pioneering theoretical work, Mühlbauer *et al* experimentally observed skyrmions for the first time in MnSi using neutron scattering under low temperature and magnetic field conditions [6]. Since then, numerous material systems, including non-centrosymmetric bulk magnets [6, 12, 13, 18, 36–41], magnetic thin films with inversion symmetry broken at interfaces [25, 42–48], centrosymmetric materials [49–53], and Van der Waals materials [50, 54, 55], have been confirmed to be able to host magnetic skyrmions. Each of these material systems possesses unique physical properties, resulting in significant variations in the size, stability, and dynamical properties of skyrmions, greatly expanding the selection range of materials for the research and application of magnetic skyrmions. A compilation of the current magnetic skyrmion material systems is presented (table 1).

### 2.1. Non-centrosymmetric bulk magnets

Skyrmions were first experimentally observed in the chiral magnet B20-type compound MnSi [6], crystallizing into a chiral cubic structure with space group $P2_13$ (figure 2(a)). Due to the absence of centrosymmetry within the crystal lattice, chiral magnets display spontaneous bulk-type DMIs (figure 1(a)). In B20 compounds, the spin configuration of magnetic skyrmions is usually the Bloch-type (figure 1(c)), owing to the influence of bulk-type DMI. In chiral magnets, bulk-type DMIs cant every neighboring spin moment direction, leading to the formation of long modulation periods of helical and skyrmion spin structures, which typically range from 10 to 100 nm.

Furthermore, the dimension of skyrmions is closely tied to the spiral period of chiral magnets, which is typically determined by the ratio of Heisenberg exchange interaction and DMI. Among chiral magnets, MnGe and $MnSi_{1-x}Ge_x$ exhibit the shortest spiral period of less than 5 nm [59, 72]. These short-period spin twists hold promise for high-density spintronic devices. However, the magnetic skyrmions in these magnets can only be stable at extremely low temperatures. FeGe [13],

**Table 1.** Summary of skyrmion type, existence conditions (temperature T and magnetic field B) and size in various magnetic skyrmions, RT means room temperature.

| Time | Materials | Skyrmion type | T (K) | B (mT) | Size (nm) | References |
|---|---|---|---|---|---|---|
| Non-centrosymmetric bulk magnets | | | | | | |
| 2009 | MnSi | Bloch | 27–29.5 | 110–220 | 19 | [6] |
| 2010 | $Fe_{0.8}Co_{0.2}Si$ | Bloch | 5–32 | 20–100 | 90 | [12] |
| 2010 | FeGe | Bloch | 100–280 | 50–250 | 70 | [13] |
| 2012 | $Cu_2OSeO_3$ | Bloch | 5–50 | 20–180 | 50 | [56] |
| 2013 | $Fe_{0.5}Co_{0.5}Si$ | Bloch | 5–30 | 25–80 | 90 | [57] |
| 2015 | Co-Zn-Mn | Bloch | 315 | 10 | 100 | [58] |
| 2015 | MnGe | Bloch | 150 | 0–2400 | 1.5 | [59] |
| 2015 | $GaV_4S_8$ | Néel | 8–13 | 20–160 | 22 | [38] |
| 2016 | $FeGe_{1-x}Si_x$ | Bloch | 95 | 130 | 50 | [60] |
| 2016 | $Fe_xCo_{1-x}Rh_{0.5}Mo_3N$ | Bloch | 20–90 | 87–149 | 100 | [61] |
| 2017 | $Mn_{1.4}Pt_{0.9}Pd_{0.1}Sn$ | Antiskyrmion | RT | 100–300 | 150 | [18] |
| 2019 | $Gd_2PdSi_3$ | Bloch | 20 | 500–1500 | 2.5 | [62] |
| 2019 | EuPtSi | Bloch | 1.8 | 800–1500 | 4 | [63] |
| 2021 | $Fe_{1.9}Ni_{0.9}Pd_{0.2}P$ | Antiskyrmion | RT | 350–450 | 100–400 | [64] |
| 2022 | $(Fe_{0.5}Co_{0.5})_5GeTe_2$ | Néel | RT | 50–150 | 200 | [65] |
| Magnetic thin-film | | | | | | |
| 2011 | Fe/Ir(111) | Néel | 11 | 0 | 1 | [66] |
| 2013 | PdFe/Ir(111) | Néel | 2.2 | 1500 | 3 | [10] |
| 2015 | Ta/CoFeB/TaOx | Néel | RT | 0.5 | 700–2000 | [45] |
| 2015 | Fe/Ni/Cu/Ni/Cu(001) | Néel | RT | 150 | 400 | [67] |
| 2016 | Ir/Co/Pt | Néel | RT | 0–80 | 40–90 | [48] |
| 2016 | Pt/Co/MgO | Néel | RT | 0–4 | 70–190 | [68] |
| 2016 | Pt/Co/Ta Pt/CoFeB/MgO | Néel | RT | 0–2 | 400–500 | [44] |
| 2017 | Ir/Fe/Pt/Co | Néel | RT | 0–150 | 40–100 | [69] |
| Other material systems | | | | | | |
| 2012 | $BaFe_{12-x-0.05}Sc_xMg_{0.05}O_{19}$ | Bloch | RT | 80–200 | 200 | [70] |
| 2014 | $La_{2-2x}Sr_{1+2x}Mn_2O_7$ | Biskyrmion | 20–46 | 350 | 200 | [22] |
| 2016 | MnNiGa | Biskyrmion | 100–340 | 400 | 90 | [49] |
| 2017 | $Fe_3Sn_2$ | Bloch | 120–630 | 700 | 300 | [71] |
| 2020 | $Fe_3GeTe_2$ | Bloch | 116 | 0–90 | 200 | [54] |

a B20 material, boasts a magnetic skyrmion phase that is stable at 280 K, the highest temperature currently observed; however, this temperature is still considered lower than room temperature. A breakthrough in the search for stable skyrmion-based devices is found in the $\beta$-Mn type Co-Zn-Mn alloy [58], a non-B20 chiral magnet with the skyrmion stable at 400 K (figure 2(b)). The discovery opens up practical potential applications of skyrmion-hosting chiral magnets.

Most chiral materials with skyrmion phases are typically metallic in nature. However, there is an exception in $Cu_2OSeO_3$, which is the first insulating material among chiral magnets and also exhibits multiferroicity [40]. Its crystal structure belongs to space group $P2_13$, similar to other B20 materials but it is more complex due to the presence of copper atoms. The appearance of skyrmions in $Cu_2OSeO_3$ is usually accompanied by alterations in macroscopic electric polarization [56]. This chiral magnet is inherently electrically insulated and multiferroic, enabling the manipulation of skyrmions through pure electric fields without causing additional Joule heating. However, the Curie temperature of $Cu_2OSeO_3$ is relatively low at approximately 58 K. Therefore, searching for other multiferroic insulating chiral magnets with a higher Curie temperature is necessary if practical applications are desired. Besides metal and insulating chiral magnetic materials, the magnetic semiconductor material $GaV_4S_8$ also exhibits skyrmion phases [38]. Notably, its skyrmion spin configuration adopts the Néel type due to the distinct symmetry of $GaV_4S_8$ from B20 compounds.

Recent studies have also reported the discovery of magnetic skyrmions in non-centrosymmetric bulk magnets with $D_{2d}$ symmetry. Two notable examples are the Heusler compounds $Mn_{1.4}PtSn$ [74, 75] and $Mn_{1.4}Pt_{0.9}Pd_{0.1}Sn$ [18, 76], in which the alteration of $D_{2d}$ symmetry impacts the symmetry of the DMI, leading to the formation of room-temperature anti-skyrmion with a size of approximately 150 nm. Noteworthily, Heusler compounds offer a wealth of options for tuning the intrinsic physical parameters that affect the skyrmion properties, such as the crystal structure, symmetry, magnetic anisotropy, and magnetic moment. As a result, these materials also demonstrate great potential for generating anti-ferromagnetic anti-skyrmions. Therefore, the discovery of anti-skyrmions in Heusler compounds has generated significant excitement in the scientific community with the potential for diverse applications.

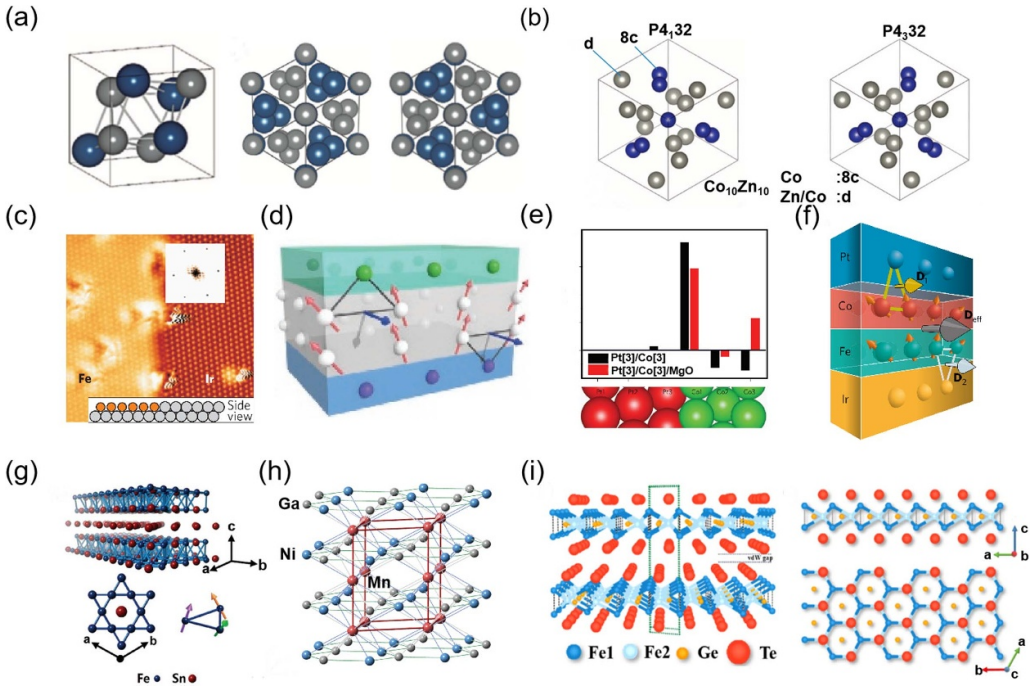


**Figure 2.** (a) Schematic diagram of the B20 chiral crystal structure of MnSi, blue atom is Mn and gray atom is Si. Reprinted with permission from [73]. Copyright (2020) American Chemical Society. (b) Schematic representation of the crystal structure of β-Mn with space groups $P4_132$ and $P4_332$, where the Co atom occupies position 8C and Zn/Co occupies position 12d. Reproduced from [58]. CC BY 4.0. (c) Atomic-resolution STM image of the pseudomorphic hexagonal Fe layer at an Ir step edge. Reproduced from [66] with permission from Springer Nature. (d) Schematic diagram of DM orientation on a single trilayer (FM, grey) consisting of a magnetic layer (FM, grey) sandwiched between two different heavy metals a (blue) and B (green). Reproduced from [48] with permission from Springer Nature. (e), Layer-resolved amplitude of the microscopic DMI for Pt[3 ML]/Co[3 ML] and Pt[3 ML]/Co[3 ML]/MgO obtained with *ab initio* calculations. Reproduced from [68] with permission from Springer Nature. (f) Schematic of multilayer stack, featuring a sequence of Ir, Fe, Co and Pt layers. The large DMI vectors at Co/Pt (top, D1) and Fe/Ir (bottom, D2) interfaces can act in concert to enhance the effective DMI. Reproduced from [69] with permission from Springer Nature. (g) Kagome magnet $Fe_3Sn_2$. [71] John Wiley & Sons. [© 2017 WILEY-VCH Verlag GmbH & Co. KGaA, Weinheim]. (h) Layered $Ni_2In$-type MnNiGa with space group P63/mmc. [49] John Wiley & Sons. [© 2016 WILEY-VCH Verlag GmbH & Co. KGaA, Weinheim]. (i) Crystal structure of a $Fe_3GeTe_2$ bilayer with an interlayer van de Waals gap. Reprinted with permission from [54]. Copyright (2020) American Chemical Society.

### 2.2. *Magnetic thin film*

In addition to the spontaneous DMI triggered by the breaking of the centrosymmetry within a crystal structure, DMI can also manifest at the interface between magnetic films and heavy metals. The absence of mirror symmetry at the magnetic film interface along with the strong SOC of heavy metals leads to an indirect exchange interaction, which is transmitted through the heavy metal atoms between two neighboring magnetic atoms. This phenomenon, referred to as interface DMI (figure 1(d)), often results in a Néel-type spin configuration of magnetic skyrmions. In 2011, Heinze *et al* made a groundbreaking discovery by identifying Néel-type skyrmions in monolayer Fe/Ir(111) [66]. Figure 2(c) depicts a scanning tunneling microscopy (STM) image of the Fe/Ir thin film structure, revealing the exceptional strength of the interface DMI, which yields skyrmion sizes as small as 1 nm, the smallest experimentally recorded to date. Furthermore, a magnetic skyrmion was subsequently observed in bilayer PdFe on the Ir(111) surface [10]. Despite the zero-field stability provided by the limited size of these skyrmions in such materials, their stable temperature usually remains below 10 K in monolayer or ultrathin magnetic films.

In recent years, magnetic skyrmion materials have been the focus of research not only in single-layer and ultrathin ferromagnetic films but also in magnetic thin film/heavy metal heterostructures and their multilayered structures grown by magnetron sputtering. In this structure, the interfacial DMI generated in the magnetic layer interface of the heavy metal stabilizes the skyrmion (figure 2(d)). Magnetron sputtering is a widely used material growth technique in industry, particularly in the field of magnetic storage. Research on magnetic skyrmions in this type of material is directly related to practical applications, promoting the application of magnetic skyrmions and generating widespread research interest. Furthermore, by controlling parameters such as film thickness and material combination, interface DMI and vertical magnetic anisotropy in this type of material can be artificially modulated. This provides great flexibility for optimizing the size, stability, and dynamic properties of magnetic skyrmions.

Currently, there are two primary material structures for magnetic thin films/heavy metal heterojunctions and their multilayer structures. The first type is the heavy metal/magnetic thin film/metal oxide structure, which includes nanoscale structures such as Pt/Co/MgO [68], Pt/CoFeB/MgO [44], and Ta/CoFeB/$TaO_x$ [45]. Recent first-principles calculations

have revealed that the interface DMIs in such structures originate not only from the interface between heavy metals (e.g. Pt and Ta) and the ferromagnetic layer but also from the interface between metal oxides and the ferromagnetic layer (figure 2(e)). First-principles calculations also indicate that the interface DMI between the ferromagnetic layer and the metal oxide interface is influenced by the charge transfer and polarization present at the interface. Furthermore, surface oxidation, as well as metal oxide, can raise the strength of DMI in such structures, leading to a reduced skyrmion size and improved stability. The heavy metal/magnetic thin film/heavy metal structure, such as the $[Ir/Co/Pt]_{10}$ multilayer structure [48], $[Pt/Co/Ta]_{15}$ multilayer structure, and Ir/Co/Fe/Pt [69] (figure 2(f)), also represent a distinct type of material structure. First-principles calculations in these structures reveal that the handedness of DMI between the two heavy metals in individual Ir/Co and Pt/Co structures is opposite; however the upper and lower surfaces in this sandwich structure (i.e. Ir/Co/Pt) ultimately provide consistent handedness of the DMI and can enhance its strength through collaborative action.

In addition to the two aforementioned structures, recent experiments have led to the observation of some unique magnetic thin film material systems, which may offer new opportunities for optimizing thin film systems. One such material system is the heterostructure of antiferromagnetic metal thin film and ferromagnetic thin film IrMn/CoFeB/MgO [77]. Experimental findings have indicated that this structure possesses a skyrmion phase. Additionally, studies have observed that the strength of the DMI in this system differs from that in other heavy metal/ferromagnetic thin film systems. However, the theoretical explanation for this phenomenon remains elusive. In magnetic thin film structures, skyrmions can exist stably at room temperature due to good vertical magnetic anisotropy. The zero-field stability of skyrmions is also guaranteed in these films. Generally, the size of magnetic skyrmions in thin film systems ranges from 100 to 1000 nm, and some experiments have indicated that they can even reach 20 nm [78]. These materials have already demonstrated promising physical properties for practical applications of skyrmions.

It has also been predicted that interfacial DMI with $C_{2v}$ symmetry can lead to formation of antiskyrmions in ultrathin magnetic films [57, 58]. In general, various types of skyrmions and antiskyrmions can be stabilized by changing the form of DMI tensor [58]. Anisotropic interfacial DMI with $C_{2v}$ symmetry has recently been realized in epitaxial Au/Co/W magnetic films [66].

### 2.3. Other material systems

Magnetic skyrmions can be produced in some centrosymmetric material systems through competition between magnetic anisotropy and magnetic dipole interactions. The discovery of these topological states in such materials has opened up new possibilities for exploring skyrmion materials. In 2017, Hou *et al* observed multiple forms and spontaneous magnetic skyrmionic bubbles in frustrated Kagome magnets $Fe_3Sn_2$ (figure 2(g)) at room temperature [71], which could be controlled in position and size by varying the external magnetic field. Similarly, biskyrmions, except for Bloch- and Néel-type skyrmions, can be produced in the centrosymmetric material $La_{2-2x}Sr_{1+2x}Mn_2O_7$ [22], Rhombohedral Rare-Earth Magnet [50, 53] and MnNiGa [49] (figure 2(h)) within a certain temperature and magnetic field range. The size of biskyrmions is typically in the range of 90–200 nm, with MnNiGa having an extremely wide temperature stability range and rich electrical properties. Furthermore, the discovery of biskyrmions in such centrosymmetric materials provides new insights for exploring new skyrmion materials due to them lacking of the DMI.

Moreover, recent studies have revealed that magnetic skyrmions can also be realized in two-dimensional Van der Waals magnetic materials. These materials offer several advantages, including easy disassembly and transfer, and also the ability to maintain long-range magnetic order even in a few or single layers. As a result, they hold immense potential for use in nanoelectronic devices. The dimensional and height integration benefits of these materials provide a strong foundation for the high-density storage of magnetic skyrmions. In 2020, Ding *et al* observed Bloch-type skyrmions in two-dimensional magnetic $Fe_3GeTe_2$ (figure 2(i)), using Lorentz transmission electron microscopy (LTEM), thereby broadening the scope of magnetic skyrmion materials to a new dimension [54]. Later, in 2022, Zhang *et al* achieved another milestone by successfully observing the existence of room-temperature skyrmions in $(Fe_{0.5}Co_{0.5})_5GeTe_2$ [65], thus greatly advancing the application process of two-dimensional skyrmion materials.

## 3. Manipulation of magnetic skyrmions

Magnetic skyrmions have garnered significant interest due to their rich physical properties and promising prospects for application. Their nanoscale size and low driven current density make them ideal information carriers in spintronic devices. However, to fully utilize skyrmions in practical devices, scientists must be able to accurately manipulate them, which includes their generation, annihilation and movement.

### 3.1. Electric current

Since the discovery of skyrmions, researchers have relentlessly explored diverse methods for manipulating them. One of the earliest and most ubiquitous methods is the use of an electric current to write, erase, and drive skyrmions. In 2013, Niklas *et al* demonstrated a noteworthy advancement by controlling the generation and annihilation of skyrmions using an STM [10]. Specifically, they injected spin-polarized currents into PdFe/Ir (111) to produce skyrmions by reducing the magnetic field from 3 T to 1.8 T and injecting higher-energy electrons through local voltage sweeps, as illustrated in figure 3(a). The researchers observed that the switching rate and direction could be tailored by modulating the current parameters. In 2014, Zhou and Ezawa proposed a device model for linking narrow nanowires with wide nanowires. Micromagnetic simulations revealed that a current could initiate the movement of magnetic DWs from narrow to wide nanowires, thus

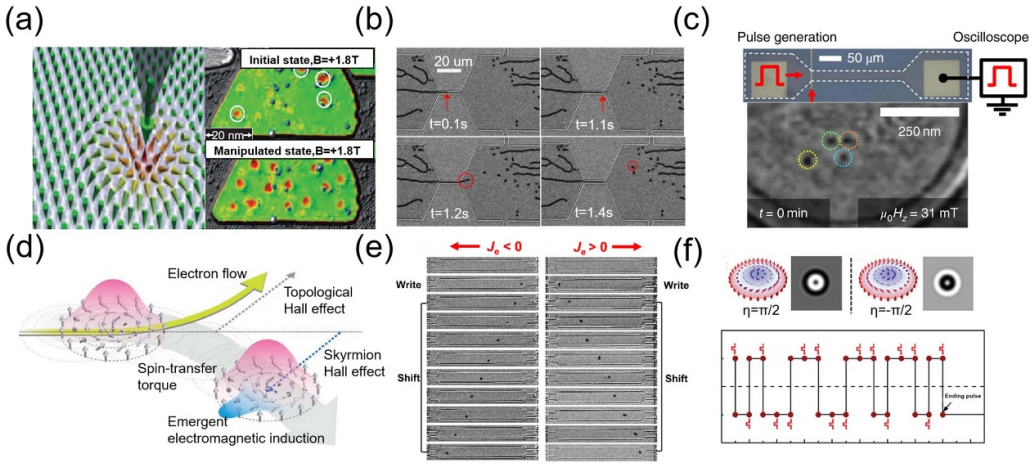


**Figure 3.** Electric current manipulation of skyrmions. (a) The concept of skyrmion manipulation using local currents from a STM tip and the SP-STM image before and after the application of spin-polarized current. From [10]. Reprinted with permission from AAAS. (b) The stripe domains are forced to pass through a constriction in the device, and are eventually converted into skyrmions on the right side of the device, as indicated by the red circles. From [45]. Reprinted with permission from AAAS. (c) The optical image of the device and the x-ray holography images of $Pt/Co_{44}Gd_{56}/TaO_x$ after current pulse. Reproduced from [80], with permission from Springer Nature. (d) The schematic picture of skyrmion motion and associated physical phenomena under the flow of electrons is depicted. The electron current drives the flow of a skyrmion by means of the spin-transfer torque mechanism. Reproduced from [15], with permission from Springer Nature. (e) The single skyrmion generation and motion driven by a current pulse for both negative and positive electron currents is shown. Reprinted with permission from [83]. Copyright (2017) American Chemical Society. (f) The schematic view of two skyrmions with opposite helicity and their corresponding simulated LTEM (Lorentz transmission Electron Microscopy) images. The images are based on the spin texture and the helicity reversal of the skyrmionic bubble with respect to the number of current pulses applied. [84] John Wiley & Sons. [© 2019 WILEY-VCH Verlag GmbH & Co. KGaA, Weinheim].

inducing the formation of skyrmions through the spin moment [79]. In 2015, Jiang *et al* confirmed these findings through experimentation. By maintaining a constant DC current of $j_e = +6.4 \times 10^4$ A cm$^{-2}$ and $B_\perp = +0.46$ mT, stripe domains were forced to traverse nanochannels, leading to contraction and resulting in the generation of skyrmions on the right side of the nanochannel, as illustrated in figure 3(b) [45]. In 2018, Lucas Caretta *et al* demonstrated spin-orbit torques (SOTs) by current induced produce small size skyrmions. As illustrated in figure 3(c), through the use of magneto-optical Kerr effect, the researchers found approach 10 nm skyrmions at room temperature in ferrimagnetic $Pt/Gd_{44}Co_{56}/TaO_X$ [80].

Recently, Liu *et al* demonstrated the generation of skyrmions through current-induced spin-orbit torques (SOTs) in a multilayer composed of $[Pt(1.5\text{ nm})/Co(1\text{ nm})/Ir(1.5\text{ nm})]_{15}$ [78]. Through the use of x-ray magnetic circular dichroism transmission microscopy, the researchers found that as current densities and SOTs increased, the size of the skyrmions decreased correspondingly, with the smallest diameter reaching approximately 20 nm [78]. These findings underscore the potential of SOTs for generating skyrmions, thus presenting another method for the manipulation and control of these non-collinear magnetic structures.

Furthermore, electric currents have been found to play a key role not only in controlling the generation and annihilation, but also movement of magnetic skyrmions. A pioneering work by Jonietz *et al* in 2010, who used neutron scattering, demonstrated that electric currents can cause the motion and rotation of skyrmions in a bulk MnSi helimagnet [81]. In 2012, Yu *et al* explored the movement of skyrmions under electrical currents in a microdevice made of the helimagnet FeGe [82] using *in-situ* LTEM, at near-room temperature. This study reported a critical current density far below 100 A cm$^{-2}$. In 2013, Nagaosa *et al* demonstrated how electric currents drive skyrmion motion through spin-transfer torques, accompanied by the Hall effect and the skyrmion Hall effect [15], as illustrated in figure 3(d). In 2017, Yu, *et al* reported the directional movement of current-driven positive and negative skyrmions in a track memory [83] (figure 3(e)). They applied a series of pulses, with a magnitude of 8 V and a duration of 10 $\mu s$ to a magnetic field of 2.7 Oe, which resulted in the successful shifting of the skyrmions. In 2020, Hou *et al* studied the dynamics of skyrmions induced by electric current in $Fe_3Sn_2$ [84]. Their study led to a remarkable discovery, namely that the application of a spin-polarized current could reverse the helicity of the skyrmions, as depicted in figure 3(f). The critical current density threshold for this effect ranged from $10^9$ to $10^{10}$ A m$^{-2}$, with a pulse width spanning from 100 to 1 ns. The authors also characterized the critical role of the pinning effect and dipole-dipole interaction in the helicity reversal process using micromagnetic simulations.

Despite the fact that the generation, annihilation and movement of skyrmions have been achieved, several challenges remain that must be addressed before their practical application. First, defects and impurities significantly impede the movement of skyrmions, leading to high actual driving current densities and energy consumption. Second, the current drive generates significant Joule heat, which is not conducive to practical applications. Finally, the movement of skyrmions is affected by the skyrmion Hall effect, which causes

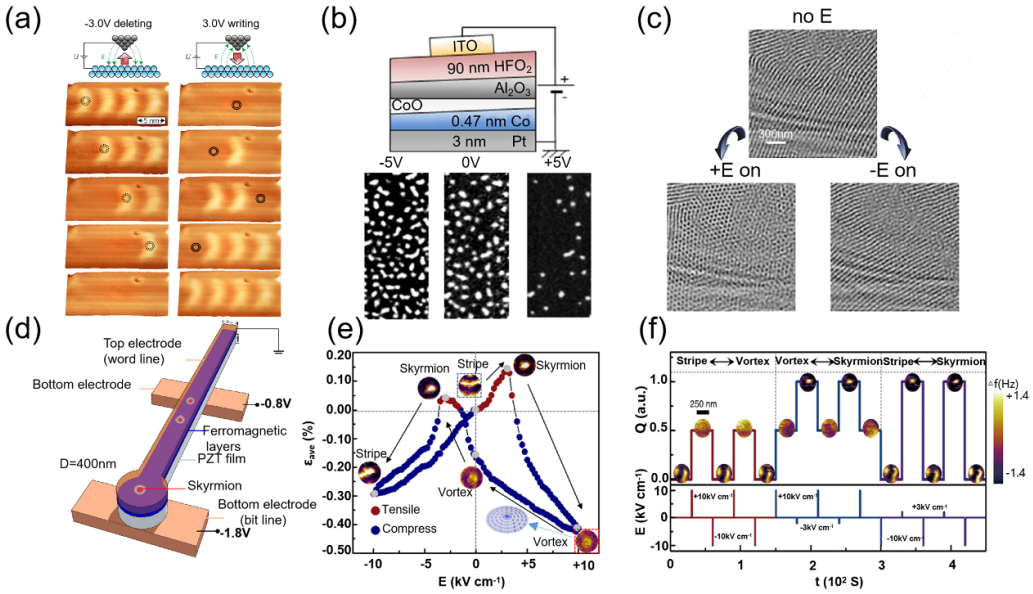


**Figure 4.** Electric field manipulation of skyrmions. (a) The experimental set-up for writing and deleting at the nanoscale, and perspective views of subsequent SP-STM constant-current images of the same area. Reproduced from [85], with permission from Springer Nature. (b) A schematic representation of the device, and Polar Kerr magnetic images that demonstrate the electric field control of skyrmion bubbles density in a Pt/Co/oxide trilayer under a static 0.15 mT perpendicular magnetic field. Reprinted with permission from [86]. Copyright (2017) American Chemical Society. (c) LTEM images that show the effect of an applied electric field on the magnetic structure of the material. An LTEM image without an electric field is compared with an image at an applied field of $E = \pm 3.6$ V $\mu$m$^{-1}$. Reprinted with permission from [89]. Copyright (2018) American Chemical Society. (d) A schematic of the simulated device structure, where a nanowire is connected to a disk with a diameter of 400 nm for skyrmion creation, propagation, and pinning. The bottom Au electrodes are applied with $-1.8$ V voltage for skyrmion creation and $-0.8$ V for skyrmion pinning, respectively. Reprinted from [90], Copyright (2018), with permission from Elsevier. (e) The transferred average strain wave and corresponding magnetic domain evolution processes in the $d \sim 350$ nm [Pt/Co/Ta]8 nano-dots in a cycle of E ranging from $+10$ kV cm$^{-1}$ to $-10$ kV cm$^{-1}$ are demonstrated. (f) Switching of the topological number Q of various magnetic domains (Q = 1.0, 0.5, and 0 correspond to skyrmion, vortex, and stripe, respectively) is achieved by applying a pulse electric field with a pulse width of 1 ms. Reproduced from [91]. CC BY 4.0.

deflected movement and reduced transmission efficiency, thereby hindering their practical application. Addressing these issues is crucial to further advance the practical use of skyrmions in various fields.

### 3.2. Electric field

The current-based manipulation of skyrmions has some inherent challenges, such as high current density, generation of excessive joule heat, and the skyrmion Hall effect. In recent years, the application of electric fields in the manipulation of skyrmions has received significant attention as it offers a promising alternative for overcoming the limitations of traditional methods. For example, in 2017, Hsu *et al* demonstrated the conversion of skyrmions in Fe/Ir (111) films through the application of voltage using a spin-polarized STM (SP-STM) needle tip [85]. By changing the electronic structure of the Fe atomic layer, the authors were able to manipulate the skyrmions, as illustrated in figure 4(a). In the same year, Schott *et al* achieved the nucleation and annihilation of skyrmions at room temperature in a Pt/Co/oxide trilayer covered by a 90 nm $HfO_2$ layer and a top indium tin oxide (ITO) electrode [86] (figure 4(b)). The authors found that the change in interface charges can alter the size of the effective magnetic anisotropy and DMI, which combined can effectively manipulate skyrmions.

In 2019, Ma *et al* leveraged a magneto-optical Kerr microscope to apply voltage to a magnetic multilayer film at room temperature. This resulted in the successful observation and realization of the electric field-induced creation and directional motion of a chiral DW and skyrmion bubbles [87]. By altering the magnetic anisotropy and size of the DMI through the application of electric fields, they were able to achieve the generation and directional movement of the magnetic DW and skyrmion.

In 2020, Bhattacharya *et al* discovered that the IrMn/CoFeB interface could produce an exchange bias magnetic field, which could serve as a substitute for the auxiliary magnetic field required for skyrmion manipulation [88]. The application of an electric field causes a change in charge at the ferromagnetic-oxide interface, leading to a significant alteration in magnetic anisotropy as well as the generation and annihilation of skyrmions in a zero magnetic field. While this electric field-based manipulation of skyrmions is effective, its application is limited to single or several layers of thin films, which restricts its broader utilization.

In the field of single-phase multiferroic materials with magneto-electric coupling, researchers have made significant advances in understanding the properties and behavior of skyrmions. In 2012, Seki *et al* discovered skyrmions in $Cu_2OSeO_3$ by using an LTEM [40]. They found that skyrmions can induce electric polarization. In 2018, Huang *et al*

used an LTEM to observe the mutual transformation between the spiral domain and skyrmion in real space under the influence of an electric field [89]. As depicted in figure 4(c), the authors observed the transition of spin helices into skyrmions by applying a voltage of 3.6 V $\mu m^{-1}$ to $Cu_2OSeO_3$.

However, despite these advances, some limitations exist to the use of single-phase multiferroic materials with magnetoelectric coupling in skyrmion manipulation. The Curie temperature of these materials is generally low, with $Cu_2OSeO_3$ having a Curie temperature of less than 65 K. This limits the practical applications of these materials in skyrmion manipulation. In recent years, FM/FE multiferroic heterostructures based on electrostriction have garnered significant research attention. In 2018, Li *et al* theoretically demonstrated the potential of these heterostructures to produce skyrmions under electric field-induced strain through micro-magnetic simulation [90], as illustrated in figure 4(d). They constructed a Pd/Fe/Ir heterostructure on a Pb $(Zr_{1-x}Ti_x)O_3$ substrate and successfully created a single stable skyrmion through applying an electric field.

In 2020, Wang *et al* conducted experimental work on an FE/FM multiferroic heterostructure that consisted of a 0.7PbMg1/3 Nb2/3O3-0.3PbTiO3 (PMN-PT) ferroelectric substrate and a $[Pt/Co/Ta]_{12}$ nanometer point [91]. They achieved polymorphic switching from stripe domains to skyrmions and vortices by applying different electric fields, as depicted in figures 4(e) and (f). These findings demonstrate the promise of FM/FE multiferroic heterostructures as a platform for electric field-based skyrmion manipulation.

### 3.3. Other methods

Apart from electrical methods, alternative techniques exist for manipulating magnetic skyrmions. One such method was demonstrated in 2013 by Finazzi *et al*, who used ultrashort single optical laser pulses to generate skyrmions in a thin ferrimagnetic film [92]. Additionally, they discovered that by adjusting the laser fluence, the topological magnetic structures could also be modified, as illustrated in figure 5(a). These topological magnetic structures were stabilized by a combination of exchange interactions and magnetic dipole-dipole interactions. In 2018, Berruto *et al* demonstrated that light-induced heat pulses of varying duration and energy can be utilized to write skyrmions in a wide range of magnetic fields and temperatures in FeGe [93]. Their experiment demonstrated that the speed at which skyrmions could be written and erased was contingent upon the cooling rate subsequent to a laser-induced temperature jump. The outcomes of their experiment are displayed in figure 5(b).

More recently, Feng *et al* discovered that the shape memory effect of a TiNiNb substrate can induce strain in [Pt/Co/Ta]n multilayers, leading to a remarkable reduction of 400 Oe in the nucleation field of the skyrmion [94]. As depicted in figures 5(c) and (d), this strain effect is attributed to a combination of plane magnetic moment rotation and a decrease in the interface DMI, as validated by theoretical simulations.

In addition to laser and stress methods, Koshibae *et al* demonstrated in 2014 that local heating can produce magnetic skyrmions in chiral and magnetic dipole magnets through theoretical simulation [95]. In 2015, Liu *et al* employed spin waves to generate skyrmions. These results have greatly expanded the methods used to manipulate magnetic skyrmions [96].

## 4. Detection of skyrmion

Although scientists can observe the existence of magnetic skyrmions through advanced technologies, such as an LTEM, their practical applications usually involve the detection of their effects on the electrical signals in spintronic devices. This can be achieved through a variety of techniques, including the detection of Hall resistance, non-collinear magnetoresistance, and tunneling magnetoresistance (TMR) in magnetic tunnel junction (MTJ) devices.

In 2016, Hamamoto *et al* introduced a method for detecting magnetic skyrmions through changes in Hall resistance. The presence of a skyrmion can be detected by observing the change in Hall resistance when it passes through a Hall bar [97]. Two years later, Maccariello *et al* successfully applied this technique to detect skyrmions in magnetic multilayers [98], as illustrated in figure 6(a).

Magnetic skyrmions exhibit a distinct non-collinear spin configuration. Due to the continuous variation of the magnetic moment of the skyrmion in space, different regions of the skyrmion display varying magnetoresistance, resulting in current fluctuations. In 2015, Hanneken *et al* proposed the use of non-collinear magnetoresistance (see figure 6(b)) as a means of detecting skyrmions [99]. Through this method, they successfully detected a single skyrmion in PdFe/Ir(111) through STM.

Due to differences in spin configuration between skyrmion and ferromagnetic states, the former generates TMR distinct from the latter when passing through MTJs. As such, MTJs offer a promising means for measuring the electrical properties of magnetic skyrmions. In fact, as early as 2015, Crum *et al* proposed that MTJ devices can be utilized to read skyrmions [100]. The movement of a skyrmion beneath the MTJ reading head causes changes in the direction of the magnetic moment, which leads to changes in related-electronic states and TMR. Such changes can be detected by observing changes in resistance values, which confirm the presence or absence of a skyrmion in the reading head area. Building on this theory, Guang *et al* successfully demonstrated the electrical read-out of magnetic skyrmions in 2022 using an MTJ device [101], as depicted in figures 6(c) and (d). They demonstrated that the electrical signal that corresponded to a single skyrmion ranged from 38 to 66 Ω, which is a significant improvement compared with the signal of detection using Hall resistance. Moreover, Li *et al* demonstrated the electrical read-out of skyrmions at room temperature using MTJ devices prepared from CoFeB/MgO thin films [102], as illustrated in figures 6(e) and (f). Overall,

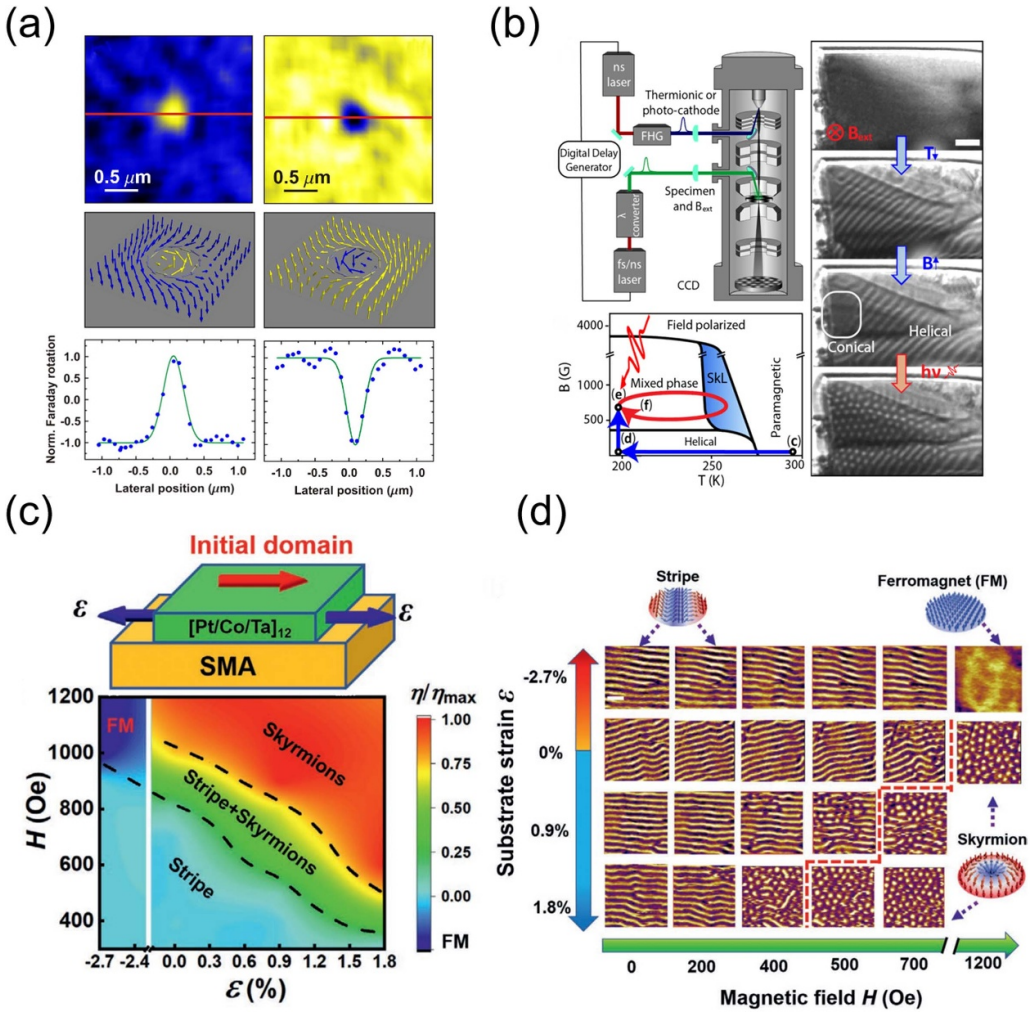


**Figure 5.** Some other methods to manipulate skyrmion. (a) Faraday rotation map displaying magnetic domains induced in a thin TbFeCo film after single laser pulse irradiation, along with corresponding skyrmion spin textures. Reprinted figure with permission from [92], Copyright (2013) by the American Physical Society. (b) The micrographs of the FeGe nanoslab and the Skyrmion lattice created by near-IR fs laser pulses. Reprinted figure with permission from [93], Copyright (2018) by the American Physical Society. (c) The sample structure and HAADF images of the as-deposited Ta(10 nm)/[Pt(3 nm)/Co(2.3 nm)/Ta(1.9 nm)]12 film. (d) Typical strain-dependent MFM images of the [Pt/Co/Ta]12 film, with the red dotted line representing the critical magnetic field at which the stripe domains transform into skyrmions. The insets show the schematic spin arrangements of different types of domains, with FM representing a ferromagnetic domain with all spins aligned parallelly. [94] John Wiley & Sons. [© 2021 Wiley-VCH GmbH].

the TMR-based detection method significantly improves the signal strength and accuracy of skyrmion detection.

## 5. Spintronic devices based on magnetic skyrmions

Following in-depth research on the properties of magnetic skyrmions, it is evident that they possess significant advantages as an information carrier, such as a high storage capacity due to their small size, sensitivity to low driving current thresholds, and reliability due to their stable structure. As a result, a range of information devices based on magnetic skyrmions have been proposed, with the application directions mainly focused on racetrack storage, logic gates, and neuromorphic devices.

### *5.1. Racetrack memory devices*

At present, hard disk drives are the most commonly used memory storage devices on the market. They use a magnetic head to move to a specific location through mechanical motion and sense changes in the magnetic field on the designated medium; thus data can be read or written. However, there is a downside to the mechanical movement, namely slow reading speeds, and external factors can also cause poor stability. These limitations mean that hard disk devices no longer meet the requirements for modern information storage. In 2008, Parkin introduced a new type of track memory that uses current-driven magnetic DW motion [103], which eliminates the need for mechanical movement. This method allows for faster reading and writing information. However, the application of track memory is limited by high drive current density and other restrictions. Fortunately,

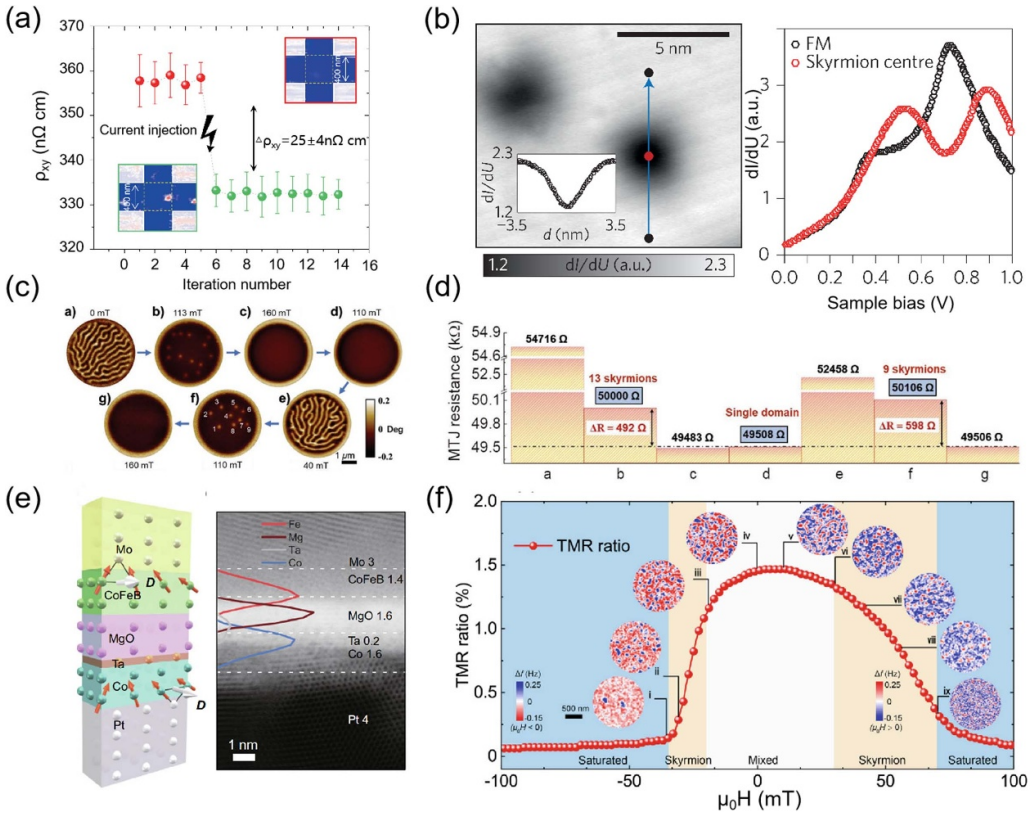


**Figure 6.** Electrical detection of skyrmions. (a) A large variation in the room temperature Hall resistivity when a single skyrmion is nucleated in the Hall cross area of a track, with red and green dots corresponding to the uniform ferromagnetic and single skyrmion states. Reproduced from [98], with permission from Springer Nature. (b) dI/dU map of two skyrmions and dI/dU tunnel spectra inside and outside a skyrmion in the FM background. Reproduced from [99], with permission from Springer Nature. (c) MFM images of domain structures in an MTJ junction with $t_{CoFeB} = 1.5$ nm and a junction size of 3 $\mu$m at different magnetic fields. (d) The resistance obtained by averaging the resistance measured before and after the MFM imaging. Reproduced from [101]. CC BY 4.0. (e) CoFeB/MgO MTJ stack structure and HAADF-STEM images of the electron energy loss spectrum (EELS) intensity. (f) TMR ratio in a magnetic field range, with the insets i–ix representing MFM images showing the nucleation and annihilation of skyrmions driven by the magnetic field. Reprinted from [102], Copyright (2022), with permission from Elsevier.

by using magnetic skyrmions instead of a DW, the drive current density can be drastically reduced, resulting in low power consumption, high density, and fast read/write times for track memory [7].

Racetrack memory devices are a type of non-volatile storage device that utilizes the magnetic DW [103, 104]. Unlike traditional magnetic memory, racetrack memory uses the magnetic domain as the magnetic storage unit. The devices responsible for storing, writing, and reading information are stationary. The movement of information along a nanowire is achieved through short pulses of spin-polarized current, and the readout device is connected to the racetrack. Since data are stored in the form of magnetic domains, it is possible to manipulate them by controlling the motion of the magnetic domains through an electric current. Magnetic skyrmions are utilized in racetrack memory and allow for the encoding of binary elementary information units (0 and 1). A skyrmion represents '1', while its absence represents '0'. Racetrack memory that uses magnetic skyrmions comprises the following four main components (figure 7(a)): a magnetic head for writing skyrmions; a nanowire used to transfer magnetic skyrmions; a read head designed to read information; and a CMOS circuit, which is responsible for generating the electric current [105]. The writing head is capable of generating a skyrmion and can define it as information '1', with its absence signifying information '0'. By activating or deactivating the writing head, the desired data can be written as '1' or '0'. During each clock cycle, a 'clock' drive pulse of constant size and duration is generated in the nanowire. This drives the electric current to act on the previously written skyrmions, transmitting them in sequence along the nanowire and forming a skyrmion sequence that contains effective information. When the skyrmion sequence passes through the read head, the previously described probing method is used to detect whether a skyrmion exists in the current bit position. In doing so, the read head is able to extract the effective information stored in the skyrmion sequence. The feasibility of this concept has been proven in experiments. In 2017, Yu *et al* designed and developed a dual-ended skyrmion track memory device [83], as illustrated in figure 7(d). By precisely adjusting the magnitude and duration of the pulse current, individual skyrmions can be generated and smoothly shifted under control.

This device brings the practical application of skyrmions significantly nearer.

Moreover, magnetic skyrmions have significant advantages in the field of racetrack memory applications. The current driving of skyrmions demonstrates a similar proportionality and speed expression to those of magnetic DWs, which have been utilized in racetrack memory. Nevertheless, due to skyrmions' unique topological properties, they have critical benefits, including a lower threshold driving current and robustness to device defects. Traditional magnetic DWs generally require a driving threshold current of between $10^{11}$ and $10^{12}$ A m$^{-2}$, whereas skyrmions' driving current theoretically only necessitates $10^{6}$ A m$^{-2}$, which is five to six orders of magnitude below that of a DW [26]. This implies that skyrmions can be precisely controlled by current. Given their small size of several nanometers, skyrmions satisfy the demands of high-density information storage [27]. Since skyrmions' motion is not impacted by the orbit shape owing to the repulsion from the boundary, they can move in curved or defective tracks. Additionally, skyrmions can bypass defects in the sample without difficulty, which eliminates concerns related to DW pinning caused by defects in racetrack memory. Furthermore, the topological stability of skyrmions helps to reduce losses and fluctuations of information in adverse conditions. The aforementioned advantages make magnetic skyrmion an attractive option for racetrack memory applications with significant potential.

In the design of spintronic racetrack memory, there are specific issues that must be considered. For example, Zhao *et al* studied two primary issues related to racetrack memory [106, 107]. The first issue is that the movement of skyrmions can be affected in actual processes by external factors, such as the temperature and non-uniformity of material grains, resulting in the misalignment of the data of the skyrmion sequence. To solve this problem, they designed a controlled magnetic anisotropy potential barrier using voltage-controlled magnetic anisotropy (VCMA), which enables the trapping and release of skyrmions in the nanoracetrack by controlling the gate. Each bit is separated by a VCMA gate, as depicted in figure 7(b), and it only opens when a skyrmion needs to pass through and closes when one needs to be read or written to. This design ensures that the entire skyrmion sequence is transmitted in a step-like manner according to the bit, avoiding misalignment due to overly fast or slow skyrmion motion.

The second problem arises from the possible errors that may occur when reading skyrmions in skyrmion-based racetrack memory. This is because in such memory, the skyrmion represents '1' and the ferromagnetic background represents '0'. If the reader fails to detect the skyrmion while reading it, this will result in errors. In addition, continuous '0' in information synchronization may cause the data to lose lock. To overcome these problems, Zhao *et al* designed a structure that uses differential coding to encode data, as illustrated in figure 7(c). In this design, two parallel nano-racetracks, L and R, connected at the leading end represent the same set of data. Both L and R have a controllable VCMA gate at the leading end, which can block or allow spin momentums to enter or exit the track. In each clock cycle, the write end generates a skyrmion according to the required data to be written, and the corresponding track is opened or closed accordingly. For example, suppose '1' is defined as a skyrmion in the R track and '0' is a skyrmion in the L track. When writing '1', the R track is opened while the L track is closed, and the skyrmion will enter the R track to form a '1' (figure 7(b)). When reading, the magnetic states of the R and L tracks must be compared differentially. If a skyrmion sequence in a track is misaligned, the two tracks will have or lack a skyrmion simultaneously during reading, which the system can immediately detect and correct. Therefore, this design greatly enhances the robustness of data in the racetrack and reduces the error rate; furthermore, because a VCMA gate can always be opened or closed at a given track, this design allows the precise control of the skyrmion sequence.

Additionally, magnetic skyrmion racetrack memory entails the problem of the skyrmion Hall effect [15, 25, 43, 109]. During movement, magnetic skyrmions may experience lateral drift due to the Magnus force (figure 3(d)), causing them to deviate from their intended path. To address this issue, Zhang *et al* suggested using synthetic antiferromagnetic skyrmions, which can eliminate the skyrmion Hall effect [108]. The magnitude and direction of the Magnus force are closely related to the topological number of the magnetic skyrmion, and they can be proportionally affected by its value. By designing an artificial antiferromagnetic layer, as depicted in figure 7(e), the magnetic moments of the magnetic skyrmion in the upper and lower ferromagnetic thin films are exactly opposite and have opposite topological numbers. Consequently, the Magnus forces acting on the two skyrmions negate each other, and their reverse magnitudes match evenly. The anti-ferromagnetic exchange coupled skyrmion pair exhibits a zero total Magnus force, making it free from the skyrmion Hall effect and allowing for precise movement in the direction of the spin polarization current. Through micromagnetic simulation (figure 7(f)), it was discovered that the skyrmion Hall effect could be effectively canceled in this structure. Furthermore, independent observations by Legrand *et al* and Dohi *et al*, have revealed the presence of skyrmions in artificial antiferromagnets [110, 111] Similarly, the skyrmion Hall effect can be eliminated in natural antiferromagnetic systems or ferromagnetic materials through angular momentum compensation points [112, 113]. To confine the movement of the skyrmion along a particular track, it has been suggested that boundary effects of the track can be enhanced by introducing highly magnetic crystalline anisotropic materials or magnetic DWs. Overall, the skyrmion Hall effect can be eliminated through the careful consideration of material selection and manipulations of the surrounding environment.

### 5.2. Logic gates

Improving modern information processing technology involves developing magnetic logic gates with a simple structure, diversified logic functions, and switchable properties. Magnetic skyrmions possess highly desirable features, including nanoscale size, topological stability, and a low driving

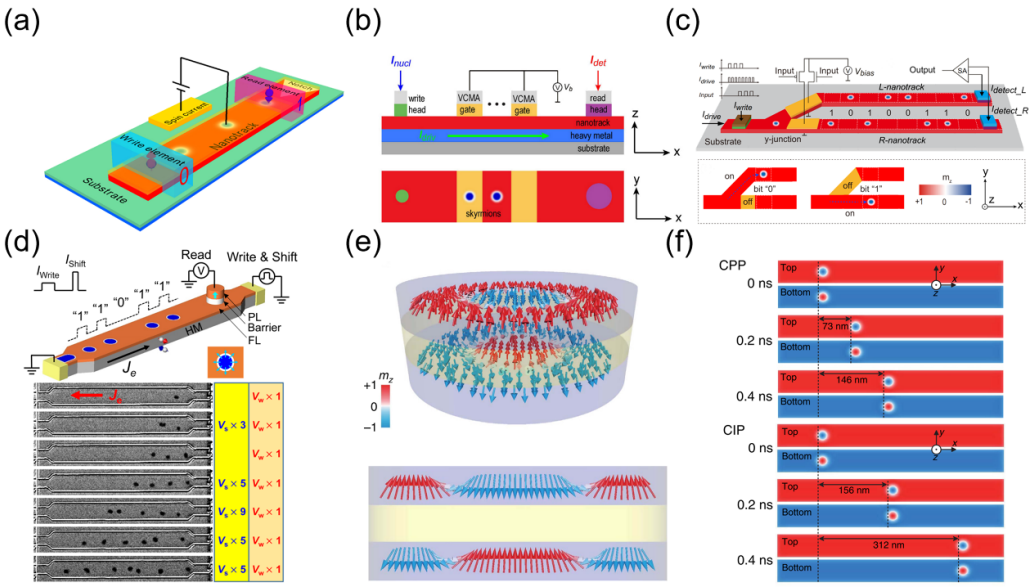


**Figure 7.** (a) Schematic diagram of the nanotrack devices using skyrmions as information carriers, this device has four main components: the writing head, the nanotrack, the reading head and the CMOS circuit for generating the spin current. Reproduced from [105], with permission from Springer Nature. (b) The schematic diagram of the VCMA skyrmionics racetrack memory. Reproduced from [106]. CC BY 4.0. (c) Schematic of the complementary skyrmion racetrack memory. © [2016] IEEE. Reprinted, with permission, from [107]. (d) Diagram of the track memory device of skyrmion at room temperature and the experimental results of controlling the production and displacement of skyrmion using current-induced spin–orbit torques. Reprinted with permission from [83]. Copyright (2017) American Chemical Society. (e) Illustration of a pair of skyrmions in an AFM-coupled nanodisk. (f) Current-induced motion of skyrmions in the top and bottom FM layers of an AFM-coupled bilayer nanotrack. Reproduced from [108]. CC BY 4.0.

threshold current, which makes them ideal for designing non-volatile, low-power consumption logic gates, which can be integrated with memory.

Zhou *et al* introduced an innovative design for logic gates using magnetic skyrmions, which can be seamlessly converted back and forth to DWs [114]. As presented in figure 8(a), by controlling the width of the nanowire, commonly used logic gates such as 'OR' and 'AND' can be realized. In a narrower nanowire, regardless of whether the input end comprises a magnetic skyrmions or both inputs are magnetic skyrmions, they will all be transformed into complete DWs. Consequently, a complete magnetic skyrmions is generated, thereby accomplishing the logical 'OR'. On the other hand, a wider nanowire produces a complete DW only when both input ends contain a magnetic skyrmion. This results in a magnetic skyrmion being obtained at the output end. However, if only one magnetic skyrmions is input, the resulting DW would not occupy the entire nanowire, creating an incomplete DW that is then absorbed by the nanowire. As a result, the logical 'AND' is achieved.

In 2022, Raab *et al* demonstrated the use of skyrmions under geometric constraints for achieving Brownian reservoir computing [116]. They designed an equilateral triangular device that contains the geometric constraints of a single skyrmion, which can be repositioned by applying different voltages to the electrodes of the triangle contact point, as illustrated in figure 8(b). By controlling the switch and limiting particle movement, they successfully demonstrated that all logic gates can be attained in a constrained geometry, as depicted in figure 8(c). The manipulation of skyrmions through geometric constraints presents promising possibilities for realizing efficient and adaptable computing operations.

Recently, Yu *et al* proposed an innovative approach for constructing skyrmions-based logic gates in a single nanotrack [117]. Their design uses a chirality barrier to achieve various magnetic skyrmion dynamic phenomena, including chirality switching, pinning, pairwise annihilation, fusion, and shunting through electric field pulses in magnetoelectric multiferroics. With the ability to control DMI chirality, this approach enables the creation of a non-volatile DMI chirality barrier for implementing and reconfiguring logic functions (figure 8(d)). This approach is particularly noteworthy for its ability to consolidate the implementation of entire logic functions into a single nanotrack, thus further simplifying the design of skyrmion-based logic devices.

### 5.3. Neuromorphic devices

Over the past ten years, neuromorphic computing has received significant attention as a cutting-edge technology that takes inspiration from the human brain's ability to store and process information. The potential of neuromorphic computing to process vast amounts of data with minimal power consumption has made it a highly sought-after technology [118–120]. The major components of a mammalian brain are synapses and neurons (figure 9(a)). Therefore, the development of neuromorphic computing that use spintronic devices focus mainly on emulating the functions of neurons and synapses [121].

Magnetic skyrmions, due to their particle-like behaviors, small size, and low driving current density, are emerging as

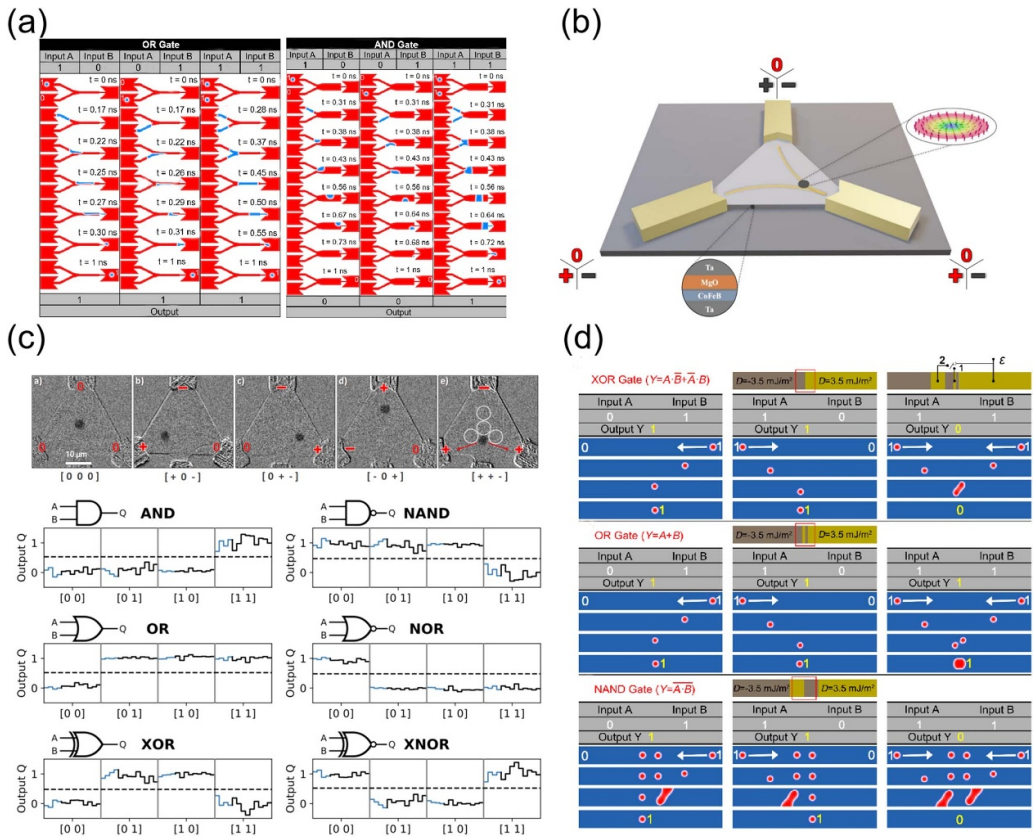


**Figure 8.** (a) 'OR' and 'AND' gate based on the conversion between skyrmions and DW pairs. Reproduced from [115]. CC BY 4.0. (b) 3D schematic of the device with different states of input modes by applying positive, negative and zero potentials. (c) Outputs of the linear read-out optimized for different Boolean operations. For each input combination ([0 0], [0 1], [1 0], [1 1]) the output Q of the linear read-out is shown for 13 sets of local skyrmion occurrence probabilities. Reproduced from [116]. CC BY 4.0. (d) Reconfigurable single-nanotrack skyrmion logic gates, including XOR gate, OR gate, NAND gate; reconfiguration can be achieved by leaving the switch vacant and flipping it to '1' and '2' respectively. The 'XNOR', 'NOR' and 'AND' functions can be reconstructed by flipping the magnetization direction of the fixed layer of magnetic tunnel junction in the above three kinds of logic gates respectively. The 'NOT' gate can be achieved by using either the left or right half of the 'NAND'. Reproduced from [117]. CC BY 4.0.

promising candidates for information carriers in neuromorphic computing design. Recently, Zhao *et al* proposed the use of magnetic skyrmions in the field of neuromorphic computing, inspired by simulating the behaviors of two key computing units in the brain-namely-synapses and neurons [28, 29]. They first designed a skyrmion-based synapse (figure 9(a)). It consists of pre- and post-synapses, both of which are located in the same nanowire ferromagnetic thin film, separated by an energy barrier with high perpendicular magnetic anisotropy (PMA) in the middle. Various means, such as DW conversion, are used to saturate the number of skyrmions in the pre-synapse. Due to the center barrier in the nanowire, all skyrmions are restricted to the pre-synapse end, forming the initial state of the synapse. When positive/negative current are introduced, skyrmions can be driven by the current to cross the energy barrier to reach or leave the post-synapse. The number of skyrmions that arrive/leave the post-synapse depends on the size and duration of the stimulus received by the device. The entire region of the post-synapse is treated as a reading area, where changes in the magnetic dipole moment can be detected using MTJs or other magnetic detectors and reflected in the form of magnetoresistance. Zhao *et al*'s study suggested that this device design can fulfill both short-term plasticity (STP) and long-term potentiation (LTP) functions in neuronal synapses simultaneously, as illustrated in figure 9(b). They also confirmed that the duration and frequency of the stimulus determine whether the device undergoes STP or LTP, consistent with synaptic design in neural networks.

A neuron is also a fundamental component of the neural networks. One of the significant properties of a neurons is that the signals in neurons are voltage-like pulses called the action potential [122]. Though the real action potentials of biological neurons exhibit complex dynamic characteristics, they can be simplified to three basic features: leak, integrate and fire. These features form the basis of the leaky-integrate-fire (LIF) neuronal model [123, 124]. Inspired by this fact, Zhao *et al* presented a neuron design that utilizes magnetic skyrmions, as illustrated in figure 9(c). This approach capitalizes on the tendency of skyrmions to move toward areas with lower energy in the gradient PMA distribution nanowire, mimicking the LIF function of a biological neuron. Their studies revealed that the skyrmion-based artificial neuron device can replicate LIF neuronal behavior (figure 9(d)).

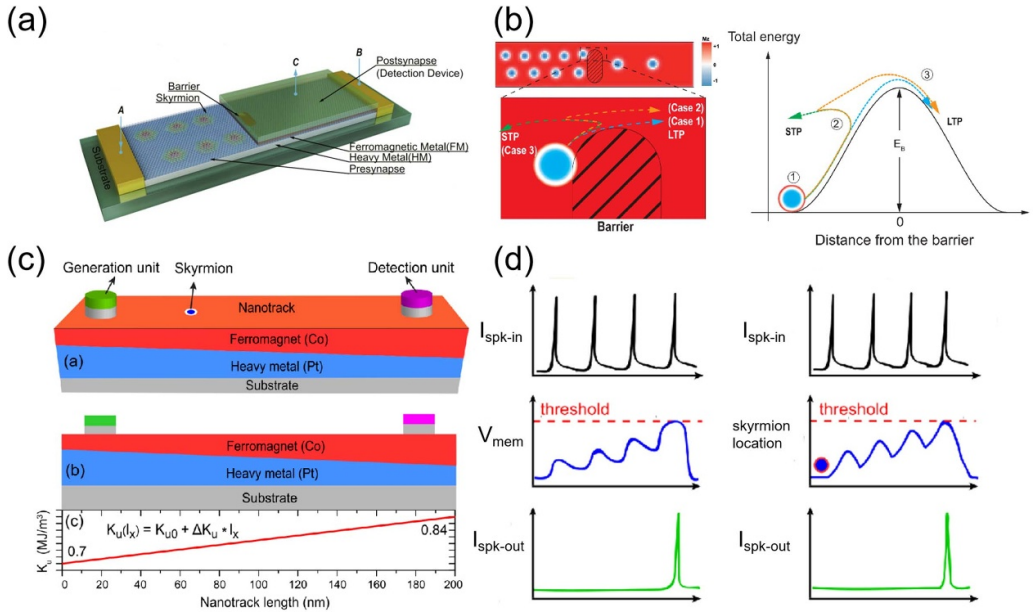


**Figure 9.** (a) Schematic of a skyrmionics synaptic devices. (b) Illustration of STP and LTP of the proposed synaptic device. Reproduced from [28]. © IOP Publishing Ltd. All rights reserved. (c) Schematic of the proposed skyrmion-based artificial neuron device and its front cross-section view. (d) The LIF behaviors of a biological neuron and a skyrmion-based artificial neuron. Reproduced from [29]. © IOP Publishing Ltd. All rights reserved.

These device designs proposed by Zhao *et al* are the first to apply magnetic skyrmions to neural network devices, thus providing a foundation for future related applications. Now, the development of skyrmion-based neuromorphic devices is breaking new ground [102, 121].

## 6. Conclusion

Since the discovery of magnetic skyrmions in experiments, research on these particle-like spin configurations has entered a period of rapid development. Various experimental materials have emerged, and investigations into the manipulation and detection of magnetic skyrmions are continuing to produce valuable insights. These promising research results have greatly advanced the fields of topological magnetism, and hold the potential to enable innovative spin electronic devices in the near future. However, significant challenges with magnetic skyrmions still require urgent attention, and thus, further fundamental research is necessary to fully unlock the potential of these fascinating particle-like spin configurations.

## 7. Future perspectives

The discovery of magnetic skyrmions has opened up promising opportunities for the development of functional spintronic memory and logic devices. In future high-density storage applications, the demand for nanoscale skyrmions with miniaturized diameters, ideally below 50 nm, is paramount. A wide range of materials capable of hosting magnetic skyrmions has been identified, with B20-type non-centrosymmetric compounds emerging as prominent candidates. The size of skyrmions in these materials spans from a few nanometers to several hundred nanometers. However, achieving stable sub-50 nm skyrmions in these materials remains challenging and limited to extremely low temperatures.

One crucial advancement lies in the utilization of the interface DMI, a robust interfacial SOC present in magnetic multilayers, enabling the realization of Néel-type skyrmions at room temperatures. Encouragingly, certain multilayer materials such as Ir/Co/Pt and Ir/Fe/Co/Pt have demonstrated the observation of sub-100 nm magnetic skyrmions at room temperature, approaching the desired range of sub-50 nm. Additionally, notable contributions from researchers, including Liu *et al*, have successfully achieved nanoscale Néel-type skyrmions through the utilization of current-induced SOTs in $[Pt(1.5\ nm)/Co(1\ nm)/Ir(1.5\ nm)]_{15}$ multilayer films [78]. By carefully tuning the current densities and associated SOTs, the size of Néel-type skyrmions can be effectively reduced, with the smallest diameter reaching approximately 20 nm at room temperature. This intriguing finding highlights the potential of precisely controlling current densities and SOTs in magnetic multilayers as a viable strategy for achieving stable sub-50 nm magnetic skyrmions at ambient conditions. Furthermore, the compatibility of magnetic multilayer materials with conventional semiconductor fabrication techniques facilitates large-scale production, rendering them crucial for driving practical applications of nanoscale skyrmionic memories and logic devices.

At the same time, the precise detection of skyrmions poses a significant challenge in the development of spin-based storage and logic devices. Currently, the primary method for accurately detecting sub-20 nm skyrmions is spin-polarized scanning tunneling microscopy. However, this technique is limited to extremely low temperatures and strong magnetic fields, rendering it unsuitable for room-temperature observations.

Recently, Liu *et al* achieved a breakthrough by successfully observing room-temperature skyrmions measuring 20 nm using x-ray magnetic circular dichroism transmission electron microscopy [78]. This achievement highlights the high precision and feasibility of this technique for studying small-scale skyrmions under near-ambient conditions. Moreover, there is a growing interest in the electrical detection of individual skyrmions for practical device applications. Nonetheless, the electrical detection of skyrmions currently faces technical barriers and necessitates further exploration and in-depth research. In the future, we anticipate making additional strides in this field to enable accurate electrical detection of extremely small magnetic skyrmions.

Meanwhile, current research on skyrmionic devices mainly focuses on manipulating a single skyrmion, including their generation, annihilation, and motion. However, these manipulation techniques fail to fully exploit the properties of skyrmions clusters and the spin chirality, which are essential for their application in advanced spintronic devices. In recent breakthroughs, our research team has achieved cascaded transitions of skyrmion clusters in a nanostructured ferromagnetic/ferroelectric multiferroic heterostructure through electric field manipulation [125]. This novel approach enables precise and continuous control over the number of skyrmions, offering non-volatile and reversible transformations critical for multi-bit memory applications. By selectively manipulating groups of skyrmions, we can realize compact and highly efficient device designs. These findings not only open new direction for the development of low-power, non-volatile, and multi-bit skyrmionic devices but also provide valuable insights into the voltage-driven control of skyrmion clusters.

Moreover, previous manipulation techniques have often neglected the quantum helicity degree of freedom inherent in skyrmions. In frustrated magnets, skyrmions exhibit a two-fold degeneracy in their Bloch-type spiral configurations (i.e. left-handed helicity and right-handed helicity) due to magnetic dipole-dipole interactions. Building upon this, Psaroudaki *et al* proposed harnessing the helicity degree of freedom in skyrmions as qubits for quantum computation [126]. Following this concept, Xia *et al* realized a qubit based on the helicity degree of freedom, enabling single-qubit quantum gates through precise control of electric fields and spin currents, while a two-qubit gate was achieved via Ising-type exchange coupling [127]. These advancements offer promising prospects for achieving universal quantum computation based on nanoscale topological spin textures.

From the existing achievements, it is evident that magnetic skyrmions will play a crucial role in the emerging field of next-generation information technology, laying the foundation for the development of spintronic devices with ultra-high storage density, ultra-fast operational speed, and ultra-low energy consumption.

## Acknowledgments

The authors thank for the financial supports from the National Key Research and Development Program of China (No. 2020YFA0309300), Science and Technology Projects in Guangzhou (202201000008), National Natural Science Foundation of China Fund (Grant Nos. 52322108, 51771127, 52171188, 52111530143 and 52271178), Science and Technology Program of Guangzhou (202002030052), Joint Research Key Fund for Guangzhou and Shen Zhen (2021B1515120047), Guangdong Basic and Applied Basic Research Foundation (2023B1515020112).

## A glossary of acronyms

A quick look-up table that define each of the whole acronyms appearing in the manuscript.

| Acronyms | Full name |
|---|---|
| SOC | Spin–orbit coupling |
| DMI | Dzyaloshinskii-Moriya interaction |
| THE | Topological Hall effect |
| RT | Room temperature |
| STM | Scanning tunneling microscopy |
| LTEM | Lorentz transmission electron microscopy |
| DC | Direct current |
| SOT | Spin-orbit torques |
| XMCD | X-ray magnetic circular dichroism |
| MOKE | Magneto-optical Kerr effect |
| DWs | Domain walls |
| SP-STM | Spin-polarized scanning tunneling microscopy |
| ITO | Indium tin oxide |
| PMN-PT | $0.7PbMg_{1/3}Nb_{2/3}O_3$-$0.3PbTiO_3$ |
| FM/FE | Ferromagnetic/ferroelectric |
| TMR | Tunneling magnetoresistance |
| MTJ | Magnetic tunnel junction |
| EELS | Electron energy loss spectrum |
| CMOS | Complementary Metal-Oxide-Semiconductor |
| VCMA | Voltage-controlled magnetic anisotropy |
| STP | Short-term plasticity |
| LTP | Long-term potentiation |
| LIF | Leaky-integrate-fire |

## ORCID iD

Zhipeng Hou https://orcid.org/0000-0003-4935-2149

## References

[1] Moore G E 1965 *Cramming more components onto integrated circuits* (New York: McGraw-Hill)
[2] Waldrop M M 2016 The chips are down for Moore's law *Nat. News* **530** 144
[3] Zhang X, Zhou Y, Mee Song K, Park T E, Xia J, Ezawa M, Liu X, Zhao W, Zhao G and Woo S 2020 Skyrmion-electronics: writing, deleting, reading and processing magnetic skyrmions toward spintronic applications *J. Phys.: Condens. Matter* **32** 143001
[4] Dzyaloshinsky I 1958 A thermodynamic theory of 'weak' ferromagnetism of antiferromagnetics *J. Phys. Chem. Solids* **4** 241
[5] Moriya T 1960 Anisotropic superexchange interaction and weak ferromagnetism *Phys. Rev.* **120** 91

[6] Mühlbauer S, Binz B, Jonietz F, Pfleiderer C, Rosch A, Neubauer A, Georgii R and Böni P 2009 Skyrmion lattice in a chiral magnet *Science* **323** 915

[7] Fert A, Cros V and Sampaio J 2013 Skyrmions on the track *Nat. Nanotechnol.* **8** 152

[8] Fert A R 1991 Magnetic and transport properties of metallic multilayers *Mater. Sci. Forum* **59–60** 439

[9] Bode M, Heide M, von Bergmann K, Ferriani P, Heinze S, Bihlmayer G, Kubetzka A, Pietzsch O, Blugel S and Wiesendanger R 2007 Chiral magnetic order at surfaces driven by inversion asymmetry *Nature* **447** 190

[10] Romming N, Hanneken C, Menzel M, Bickel J E, Wolter B, von Bergmann K, Kubetzka A and Wiesendanger R 2013 Writing and deleting single magnetic skyrmions *Science* **341** 636

[11] Everschor-Sitte K and Sitte M 2014 Real-space Berry phases: skyrmion soccer *J. Appl. Phys.* **115** 172602

[12] Yu X Z, Onose Y, Kanazawa N, Park J H, Han J H, Matsui Y, Nagaosa N and Tokura Y 2010 Real-space observation of a two-dimensional skyrmion crystal *Nature* **465** 901

[13] Yu X Z, Kanazawa N, Onose Y, Kimoto K, Zhang W Z, Ishiwata S, Matsui Y and Tokura Y 2011 Near room-temperature formation of a skyrmion crystal in thin-films of the helimagnet FeGe *Nat. Mater.* **10** 106

[14] Tonomura A, Yu X, Yanagisawa K, Matsuda T, Onose Y, Kanazawa N, Park H S and Tokura Y 2012 Real-space observation of skyrmion lattice in helimagnet MnSi thin samples *Nano Lett.* **12** 1673

[15] Nagaosa N and Tokura Y 2013 Topological properties and dynamics of magnetic skyrmions *Nat. Nanotechnol.* **8** 899

[16] Bogdanov A and Yablonskiui D 1989 Thermodynamically stable 'vortices' in magnetically ordered crystals. The mixed state of magnets *Sov. Phys.—JETP* **68** 101

[17] Bogdanov A N, Rößler U K, Wolf M and Müller K-H 2002 Magnetic structures and reorientation transitions in noncentrosymmetric uniaxial antiferromagnets *Phys. Rev.* B **66** 214410

[18] Nayak A K, Kumar V, Ma T, Werner P, Pippel E, Sahoo R, Damay F, Rossler U K, Felser C and Parkin S S P 2017 Magnetic antiskyrmions above room temperature in tetragonal Heusler materials *Nature* **548** 561

[19] Koshibae W and Nagaosa N 2016 Theory of antiskyrmions in magnets *Nat. Commun.* **7** 10542

[20] Kuchkin V M and Kiselev N S 2020 Turning a chiral skyrmion inside out *Phys. Rev.* B **101** 064408

[21] Zheng F, Kiselev N S, Yang L, Kuchkin V M, Rybakov F N, Blügel S and Dunin-Borkowski R E 2022 Skyrmion–antiskyrmion pair creation and annihilation in a cubic chiral magnet *Nat. Phys.* **18** 863

[22] Yu X Z, Tokunaga Y, Kaneko Y, Zhang W Z, Kimoto K, Matsui Y, Taguchi Y and Tokura Y 2014 Biskyrmion states and their current-driven motion in a layered manganite *Nat. Commun.* **5** 3198

[23] Yu X Z, Koshibae W, Tokunaga Y, Shibata K, Taguchi Y, Nagaosa N and Tokura Y 2018 Transformation between meron and skyrmion topological spin textures in a chiral magnet *Nature* **564** 95

[24] Bruno P, Dugaev V K and Taillefumier M 2004 Topological Hall effect and Berry phase in magnetic nanostructures *Phys. Rev. Lett.* **93** 096806

[25] Jiang W *et al* 2016 Direct observation of the skyrmion Hall effect *Nat. Phys.* **13** 162

[26] Schulz T, Ritz R, Bauer A, Halder M, Wagner M, Franz C, Pfleiderer C, Everschor K, Garst M and Rosch A 2012 Emergent electrodynamics of skyrmions in a chiral magnet *Nat. Phys.* **8** 301

[27] Romming N, Kubetzka A, Hanneken C, von Bergmann K, Wiesendanger R and von Bergmann K 2015 Field-dependent size and shape of single magnetic skyrmions *Phys. Rev. Lett.* **114** 177203

[28] Li S, Kang W, Huang Y, Zhang X, Zhou Y and Zhao W 2017 Magnetic skyrmion-based artificial neuron device *Nanotechnology* **28** 31lt01

[29] Huang Y, Kang W, Zhang X, Zhou Y and Zhao W 2017 Magnetic skyrmion-based synaptic devices *Nanotechnology* **28** 08LT02

[30] Skyrme T H R 1962 A unified field theory of mesons and baryons *Nucl. Phys.* **31** 556

[31] Sondhi S L, Karlhede A, Kivelson S A and Rezayi E H 1993 Skyrmions and the crossover from the integer to fractional quantum Hall effect at small Zeeman energies *Phys. Rev.* B **47** 16419

[32] Abolfath M, Palacios J J, Fertig H A, Girvin S M and MacDonald A H 1997 Skrymions in quantum Hall systems *Phys. Rev.* B **56** 6795

[33] Wright D C and Mermin N D 1989 Crystalline liquids: the blue phases *Rev. Mod. Phys.* **61** 385

[34] Ho T-L 1998 Spinor Bose condensates in optical traps *Phys. Rev. Lett.* **81** 742

[35] Rößler U K, Bogdanov A and Pfleiderer C 2006 Spontaneous skyrmion ground states in magnetic metals *Nature* **442** 797

[36] Karube K *et al* 2018 Disordered skyrmion phase stabilized by magnetic frustration in a chiral magnet *Sci. Adv.* **4** eaar7043

[37] Chacon A, Heinen L, Halder M, Bauer A, Simeth W, Mühlbauer S, Berger H, Garst M, Rosch A and Pfleiderer C 2018 Observation of two independent skyrmion phases in a chiral magnetic material *Nat. Phys.* **14** 936

[38] Kézsmárki I *et al* 2015 Néel-type skyrmion lattice with confined orientation in the polar magnetic semiconductor GaV4S8 *Nat. Mater.* **14** 1116

[39] Karube K, White J S, Morikawa D, Bartkowiak M, Kikkawa A, Tokunaga Y, Arima T, Rønnow H M, Tokura Y and Taguchi Y 2017 Skyrmion formation in a bulk chiral magnet at zero magnetic field and above room temperature *Phys. Rev. Mater.* **1** 074405

[40] Seki S, Yu X Z, Ishiwata S and Tokura Y 2012 Observation of skyrmions in a multiferroic material *Science* **336** 198

[41] Shibata K, Yu X Z, Hara T, Morikawa D, Kanazawa N, Kimoto K, Ishiwata S, Matsui Y and Tokura Y 2013 Towards control of the size and helicity of skyrmions in helimagnetic alloys by spin-orbit coupling *Nat. Nanotechnol.* **8** 723

[42] Buttner F *et al* 2017 Field-free deterministic ultrafast creation of magnetic skyrmions by spin-orbit torques *Nat. Nanotechnol.* **12** 1040

[43] Litzius K *et al* 2017 Skyrmion Hall effect revealed by direct time-resolved x-ray microscopy *Nat. Phys.* **13** 170

[44] Woo S *et al* 2016 Observation of room-temperature magnetic skyrmions and their current-driven dynamics in ultrathin metallic ferromagnets *Nat. Mater.* **15** 501

[45] Jiang W *et al* 2015 Blowing magnetic skyrmion bubbles *Science* **349** 283

[46] Wang K, Qian L, Chen W, Ying S-C, Xiao G and Wu X 2019 Spin torque effect on topological defects and transitions of magnetic domain phases in Ta/CoFeB/MgO *Phys. Rev.* B **99** 184410

[47] Wang K, Zhang Y, Bheemarasetty V, Zhou S, Ying S-C and Xiao G 2022 Single skyrmion true random number generator using local dynamics and interaction between skyrmions *Nat. Commun.* **13** 722

[48] Moreau-Luchaire C *et al* 2016 Additive interfacial chiral interaction in multilayers for stabilization of small individual skyrmions at room temperature *Nat. Nanotechnol.* **11** 444

[49] Wang W *et al* 2016 A centrosymmetric hexagonal magnet with superstable biskyrmion magnetic nanodomains in a wide temperature range of 100–340 K *Adv. Mater.* **28** 6887

[50] Yasui Y *et al* 2020 Imaging the coupling between itinerant electrons and localised moments in the centrosymmetric skyrmion magnet $GdRu_2Si_2$ *Nat. Commun.* **11** 5925

[51] Khanh N D *et al* 2020 Nanometric square skyrmion lattice in a centrosymmetric tetragonal magnet *Nat. Nanotechnol.* **15** 444

[52] Paddison J A, Rai B K, May A F, Calder S, Stone M B, Frontzek M D and Christianson A D 2022 Magnetic interactions of the centrosymmetric skyrmion material $Gd_2PdSi_3$ *Phys. Rev. Lett.* **129** 137202

[53] Zuo S, Qiao K, Zhang Y, Zhao T, Jiang C and Shen B 2023 Spontaneous biskyrmion lattice in a centrosymmetric rhombohedral rare-earth magnet with easy-plane anisotropy *Nano Lett.* **23** 550

[54] Ding B, Li Z, Xu G, Li H, Hou Z, Liu E, Xi X, Xu F, Yao Y and Wang W 2019 Observation of magnetic skyrmion bubbles in a van der Waals ferromagnet $Fe_3GeTe_2$ *Nano Lett.* **20** 868

[55] Zhang C *et al* 2022 Magnetic skyrmions with unconventional helicity polarization in a Van Der Waals ferromagnet *Adv. Mater.* **34** 2204163

[56] Onose Y, Okamura Y, Seki S, Ishiwata S and Tokura Y 2012 Observation of magnetic excitations of skyrmion crystal in a helimagnetic insulator $Cu_2OSeO_3$ *Phys. Rev. Lett.* **109** 037603

[57] Milde P *et al* 2013 Unwinding of a skyrmion lattice by magnetic monopoles *Science* **340** 1076

[58] Tokunaga Y, Yu X, White J, Rønnow H M, Morikawa D, Taguchi Y and Tokura Y 2015 A new class of chiral materials hosting magnetic skyrmions beyond room temperature *Nat. Commun.* **6** 1

[59] Tanigaki T, Shibata K, Kanazawa N, Yu X, Onose Y, Park H S, Shindo D and Tokura Y 2015 Real-space observation of short-period cubic lattice of skyrmions in MnGe *Nano Lett.* **15** 5438

[60] Matsumoto T, So Y-G, Kohno Y, Sawada H, Ikuhara Y and Shibata N 2016 Direct observation of $\Sigma 7$ domain boundary core structure in magnetic skyrmion lattice *Sci. Adv.* **2** e1501280

[61] Li W, Jin C, Che R, Wei W, Lin L, Zhang L, Du H, Tian M and Zang J 2016 Emergence of skyrmions from rich parent phases in the molybdenum nitrides *Phys. Rev.* B **93** 060409

[62] Kurumaji T, Nakajima T, Hirschberger M, Kikkawa A, Yamasaki Y, Sagayama H, Nakao H, Taguchi Y, Arima T-H and Tokura Y 2019 Skyrmion lattice with a giant topological Hall effect in a frustrated triangular-lattice magnet *Science* **365** 914

[63] Kaneko K *et al* 2019 Unique helical magnetic order and field-induced phase in trillium lattice antiferromagnet EuPtSi *J. Phys. Soc. Japan* **88** 013702

[64] Karube K, Peng L, Masell J, Yu X, Kagawa F, Tokura Y and Taguchi Y 2021 Room-temperature antiskyrmions and sawtooth surface textures in a non-centrosymmetric magnet with $S_4$ symmetry *Nat. Mater.* **20** 335

[65] Zhang H *et al* 2022 Room-temperature skyrmion lattice in a layered magnet $(Fe_{0.5}Co_{0.5})_5GeTe_2$ *Sci. Adv.* **8** eabm7103

[66] Heinze S, Von Bergmann K, Menzel M, Brede J, Kubetzka A, Wiesendanger R, Bihlmayer G and Blügel S 2011 Spontaneous atomic-scale magnetic skyrmion lattice in two dimensions *Nat. Phys.* **7** 713

[67] Chen G, Mascaraque A, N'Diaye A T and Schmid A K 2015 Room temperature skyrmion ground state stabilized through interlayer exchange coupling *Appl. Phys. Lett.* **106** 242404

[68] Boulle O *et al* 2016 Room-temperature chiral magnetic skyrmions in ultrathin magnetic nanostructures *Nat. Nanotechnol.* **11** 449

[69] Soumyanarayanan A *et al* 2017 Tunable room-temperature magnetic skyrmions in Ir/Fe/Co/Pt multilayers *Nat. Mater.* **16** 898

[70] Yu X, Mostovoy M, Tokunaga Y, Zhang W, Kimoto K, Matsui Y, Kaneko Y, Nagaosa N and Tokura Y 2012 Magnetic stripes and skyrmions with helicity reversals *Proc. Natl Acad. Sci.* **109** 8856

[71] Hou Z *et al* 2017 Observation of various and spontaneous magnetic skyrmionic bubbles at room temperature in a frustrated kagome magnet with uniaxial magnetic anisotropy *Adv. Mater.* **29** 1701144

[72] Makarova O L, Tsvyashchenko A V, Andre G, Porcher F, Fomicheva L N, Rey N and Mirebeau I 2012 Neutron diffraction study of the chiral magnet MnGe *Phys. Rev.* B **85** 205205

[73] Tokura Y and Kanazawa N 2020 Magnetic skyrmion materials *Chem. Rev.* **121** 2857

[74] Vir P, Kumar N, Borrmann H, Jamijansuren B, Kreiner G, Shekhar C and Felser C 2019 Tetragonal superstructure of the antiskyrmion hosting heusler compound $Mn_{1.4}PtSn$ *Chem. Mater.* **31** 5876

[75] Ma T, Sharma A K, Saha R, Srivastava A K, Werner P, Vir P, Kumar V, Felser C and Parkin S S P 2020 Tunable magnetic antiskyrmion size and helical period from nanometers to micrometers in a D(2d) heusler compound *Adv. Mater.* **32** e2002043

[76] Peng L, Takagi R, Koshibae W, Shibata K, Nakajima K, Arima T-H, Nagaosa N, Seki S, Yu X and Tokura Y 2020 Controlled transformation of skyrmions and antiskyrmions in a non-centrosymmetric magnet *Nat. Nanotechnol.* **15** 181

[77] Yu G *et al* 2018 Room-temperature skyrmions in an antiferromagnet-based heterostructure *Nano Lett.* **18** 980

[78] Liu J, Wang Z, Xu T, Zhou H, Zhao L, Je S-G, Im M-Y, Fang L and Jiang W 2022 The 20 nm skyrmion generated at room temperature by spin-orbit torques *Chin. Phys. Lett.* **39** 017501

[79] Zhou Y and Ezawa M 2014 A reversible conversion between a skyrmion and a domain-wall pair in a junction geometry *Nat. Commun.* **5** 4652

[80] Caretta L *et al* 2018 Fast current-driven domain walls and small skyrmions in a compensated ferrimagnet *Nat. Nanotechnol.* **13** 1154

[81] Jonietz F *et al* 2010 Spin transfer torques in MnSi at ultralow current densities *Science* **330** 1648

[82] Yu X Z, Kanazawa N, Zhang W Z, Nagai T, Hara T, Kimoto K, Matsui Y, Onose Y and Tokura Y 2012 Skyrmion flow near room temperature in an ultralow current density *Nat. Commun.* **3** 988

[83] Yu G *et al* 2017 Room-temperature skyrmion shift device for memory application *Nano Lett.* **17** 261

[84] Hou Z *et al* 2020 Current-induced helicity reversal of a single skyrmionic bubble Chain in a nanostructured frustrated magnet *Adv. Mater.* **32** e1904815

[85] Hsu P-J, Kubetzka A, Finco A, Romming N, von Bergmann K and Wiesendanger R 2016 Electric-field-driven switching of individual magnetic skyrmions *Nat. Nanotechnol.* **12** 123

[86] Schott M, Bernand-Mantel A, Ranno L, Pizzini S, Vogel J, Bea H, Baraduc C, Auffret S, Gaudin G and Givord D 2017 The skyrmion switch: turning magnetic skyrmion bubbles on and off with an electric field *Nano Lett.* **17** 3006

[87] Ma C, Zhang X, Xia J, Ezawa M, Jiang W, Ono T, Piramanayagam S N, Morisako A, Zhou Y and Liu X

2019 Electric field-induced creation and directional motion of domain walls and skyrmion bubbles *Nano Lett.* **19** 353
[88] Bhattacharya D, Razavi S A, Wu H, Dai B, Wang K L and Atulasimha J 2020 Creation and annihilation of non-volatile fixed magnetic skyrmions using voltage control of magnetic anisotropy *Nat. Electron.* **3** 539
[89] Huang P, Cantoni M, Kruchkov A, Rajeswari J, Magrez A, Carbone F and Rønnow H M 2018 *In situ* electric field skyrmion creation in magnetoelectric CuOSeO *Nano Lett.* **18** 5167
[90] Li Z, Zhang Y, Huang Y, Wang C, Zhang X, Liu Y, Zhou Y, Kang W, Koli S C and Lei N 2018 Strain-controlled skyrmion creation and propagation in ferroelectric/ferromagnetic hybrid wires *J. Magn. Magn. Mater.* **455** 19
[91] Wang Y *et al* 2020 Electric-field-driven non-volatile multi-state switching of individual skyrmions in a multiferroic heterostructure *Nat. Commun.* **11** 3577
[92] Finazzi M, Savoini M, Khorsand A R, Tsukamoto A, Itoh A, Duo L, Kirilyuk A, Rasing T and Ezawa M 2013 Laser-induced magnetic nanostructures with tunable topological properties *Phys. Rev. Lett.* **110** 177205
[93] Berruto G *et al* 2018 Laser-induced skyrmion writing and erasing in an ultrafast cryo-lorentz transmission electron microscope *Phys. Rev. Lett.* **120** 117201
[94] Feng C *et al* 2021 Field-free manipulation of skyrmion creation and annihilation by tunable strain engineering *Adv. Funct. Mater.* **31** 2008715
[95] Koshibae W and Nagaosa N 2014 Creation of skyrmions and antiskyrmions by local heating *Nat. Commun.* **5** 5148
[96] Liu Y, Yin G, Zang J, Shi J and Lake R K 2015 Skyrmion creation and annihilation by spin waves *Appl. Phys. Lett.* **107** 152411
[97] Hamamoto K, Ezawa M and Nagaosa N 2016 Purely electrical detection of a skyrmion in constricted geometry *Appl. Phys. Lett.* **108** 112401
[98] Maccariello D, Legrand W, Reyren N, Garcia K, Bouzehouane K, Collin S, Cros V and Fert A 2018 Electrical detection of single magnetic skyrmions in metallic multilayers at room temperature *Nat. Nanotechnol.* **13** 233
[99] Hanneken C, Otte F, Kubetzka A, Dupe B, Romming N, von Bergmann K, Wiesendanger R and Heinze S 2015 Electrical detection of magnetic skyrmions by tunnelling non-collinear magnetoresistance *Nat. Nanotechnol.* **10** 1039
[100] Crum D M, Bouhassoune M, Bouaziz J, Schweflinghaus B, Blugel S and Lounis S 2015 Perpendicular reading of single confined magnetic skyrmions *Nat. Commun.* **6** 8541
[101] Guang Y *et al* 2022 Electrical detection of magnetic skyrmions in a magnetic tunnel junction *Adv. Electron. Mater.* **9** 2200570
[102] Li S *et al* 2022 Experimental demonstration of skyrmionic magnetic tunnel junction at room temperature *Sci. Bull.* **67** 691
[103] Parkin S S P, Hayashi M and Thomas L 2008 Magnetic domain-wall racetrack memory *Science* **320** 190
[104] Parkin S and Yang S-H 2015 Memory on the racetrack *Nat. Nanotechnol.* **10** 195
[105] Zhang X, Zhao G P, Fangohr H, Liu J P, Xia W X, Xia J and Morvan F J 2015 Skyrmion-skyrmion and skyrmion-edge repulsions in skyrmion-based racetrack memory *Sci. Rep.* **5** 7643
[106] Kang W, Huang Y, Zheng C, Lv W, Lei N, Zhang Y, Zhang X, Zhou Y and Zhao W 2016 Voltage controlled magnetic skyrmion motion for racetrack memory *Sci. Rep.* **6** 23164
[107] Kang W, Zheng C, Huang Y, Zhang X, Zhou Y, Lv W and Zhao W 2016 Complementary skyrmion racetrack memory with voltage manipulation *IEEE Electr. Device. Lett.* **37** 924
[108] Zhang X, Zhou Y and Ezawa M 2016 Magnetic bilayer-skyrmions without skyrmion Hall effect *Nat. Commun.* **7** 10293
[109] Zang J, Mostovoy M, Han J H and Nagaosa N 2011 Dynamics of skyrmion crystals in metallic thin films *Phys. Rev. Lett.* **107** 136804
[110] Legrand W, Maccariello D, Ajejas F, Collin S, Vecchiola A, Bouzehouane K, Reyren N, Cros V and Fert A 2020 Room-temperature stabilization of antiferromagnetic skyrmions in synthetic antiferromagnets *Nat. Mater.* **19** 34
[111] Dohi T, DuttaGupta S, Fukami S and Ohno H 2019 Formation and current-induced motion of synthetic antiferromagnetic skyrmion bubbles *Nat. Commun.* **10** 5153
[112] Shiino T, Oh S-H, Haney P M, Lee S-W, Go G, Park B-G and Lee K-J 2016 Antiferromagnetic domain wall motion driven by spin-orbit torques *Phys. Rev. Lett.* **117** 087203
[113] Zhang X, Zhou Y and Ezawa M 2016 Antiferromagnetic skyrmion: stability, creation and manipulation *Sci. Rep.* **6** 24795
[114] Zhang X, Zhou Y, Ezawa M, Zhao G P and Zhao W 2015 Magnetic skyrmion transistor: skyrmion motion in a voltage-gated nanotrack *Sci. Rep.* **5** 11369
[115] Zhang X, Ezawa M and Zhou Y 2015 Magnetic skyrmion logic gates: conversion, duplication and merging of skyrmions *Sci. Rep.* **5** 9400
[116] Raab K, Brems M A, Beneke G, Dohi T, Rothorl J, Kammerbauer F, Mentink J H and Klaui M 2022 Brownian reservoir computing realized using geometrically confined skyrmion dynamics *Nat. Commun.* **13** 6982
[117] Yu D, Yang H, Chshiev M and Fert A 2022 Skyrmions-based logic gates in one single nanotrack completely reconstructed via chirality barrier *Nat. Sci. Rev.* **9** 12
[118] Locatelli N, Cros V and Grollier J 2014 Spin-torque building blocks *Nat. Mater.* **13** 11
[119] Grollier J, Querlioz D and Stiles M D 2016 Spintronic nanodevices for bioinspired computing *Proc. IEEE* **104** 2024
[120] Zhou J and Chen J 2021 Prospect of spintronics in neuromorphic computing *Adv. Electron. Mater.* **7** 2100465
[121] Song K M *et al* 2020 Skyrmion-based artificial synapses for neuromorphic computing *Nat. Electron.* **3** 148
[122] Hodgkin A L and Huxley A F 1952 A quantitative description of membrane current and its application to conduction and excitation in nerve *J. Physiol.* **117** 500
[123] Izhikevich E M 2003 Simple model of spiking neurons *IEEE Trans. Neural Netw.* **14** 1569
[124] Ghosh-Dastiday S and Adeli H 2009 Spiking neural networks *Int. J. Neural Syst.* **19** 295
[125] Hou Z *et al* 2022 Controlled switching of the number of skyrmions in a magnetic nanodot by electric fields *Adv. Mater.* **34** e2107908
[126] Psaroudaki C and Panagopoulos C 2021 Skyrmion qubits: a new class of quantum logic elements based on nanoscale magnetization *Phys. Rev. Lett.* **127** 067201
[127] Xia J, Zhang X, Liu X, Zhou Y and Ezawa M 2023 Universal quantum computation based on nanoscale skyrmion helicity qubits in frustrated magnets *Phys. Rev. Lett.* **130** 106701